
Diffusion Bridge Implicit Models

Kaiwen Zheng^{†1*}, Guande He^{†1*}, Jianfei Chen¹, Fan Bao¹², Jun Zhu^{‡123}

¹Dept. of Comp. Sci. & Tech., Institute for AI, BNRist Center, THBI Lab

¹Tsinghua-Bosch Joint ML Center, Tsinghua University, Beijing, China

²Shengshu Technology, Beijing ³Pazhou Lab (Huangpu), Guangzhou, China

zkwthu@gmail.com; guande.he17@outlook.com;

bf19@mails.tsinghua.edu.cn; {jianfeic, dcszj}@tsinghua.edu.cn

Abstract

Denosing diffusion bridge models (DDBMs) are a powerful variant of diffusion models for interpolating between two arbitrary paired distributions given as endpoints. Despite their promising performance in tasks like image translation, DDBMs require a computationally intensive sampling process that involves the simulation of a (stochastic) differential equation through hundreds of network evaluations. In this work, we present diffusion bridge implicit models (DBIMs) for accelerated sampling of diffusion bridges without extra training. We generalize DDBMs via a class of non-Markovian diffusion bridges defined on the discretized timesteps concerning sampling, which share the same training objective as DDBMs. These generalized diffusion bridges give rise to generative processes ranging from stochastic to deterministic (i.e., an implicit probabilistic model) while being up to $25\times$ faster than the vanilla sampler of DDBMs. Moreover, the deterministic sampling procedure yielded by DBIMs enables faithful encoding and reconstruction by a booting noise used in the initial sampling step, and allows us to perform semantically meaningful interpolation in image translation tasks by regarding the booting noise as the latent variable.

1 Introduction

Diffusion models [44, 38, 16] represent a family of powerful generative models, with high-quality generation ability, stable training, and scalability to high dimensions. They have consistently obtained state-of-the-art performance in various domains, including image synthesis [10, 21], speech and video generation [5, 15], controllable image manipulation [32–34, 30], density estimation [43, 24, 27, 52] and inverse problem solving [7, 22]. They also act as fundamental components of modern text-to-image [34] and text-to-video [13, 1] synthesis systems, ushering in the era of AI-generated content.

However, diffusion models are not well-suited for solving tasks like image translation or restoration, where the transport between two arbitrary probability distributions is to be modeled given paired endpoints. Diffusion models are rooted in a stochastic process that gradually transforms between data and noise, and the prior distribution is typically restricted to the “non-informative” random Gaussian noises. Adapting diffusion models to scenarios where a more informative prior naturally exists, such as image translation/restoration, requires cumbersome techniques like adding conditions to the model [17, 35], modifying the generation pipeline [30, 45] or adding extra guidance terms during sampling [7, 22]. These approaches inevitably result in either sub-par performance or slow and resource-intensive inference processes.

Recently, denosing diffusion bridge models (DDBMs) [53] have emerged as a scalable and promising approach to solving the distribution translation tasks. By considering the reverse-time processes of

*Work done during an internship at Shengshu; [†]Equal contribution; [‡]The corresponding author.

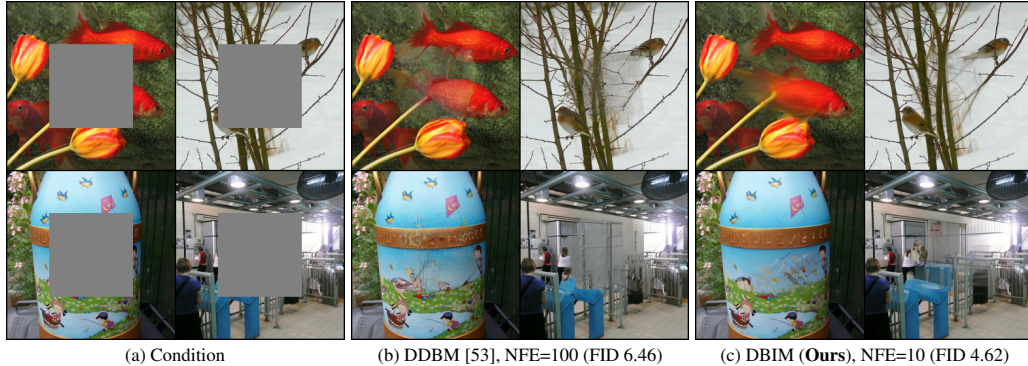


Figure 1: Inpainting results on the ImageNet 256×256 dataset [9] by DDBM [53] with 100 number of function evaluations (NFE), and DBIM (ours) with only 10 NFE.

a diffusion bridge, which represent diffusion processes conditioned on given endpoints, DDBMs offer a general framework for distribution translation. While excelling in image translation tasks with exceptional quality and fidelity, sampling from DDBMs requires simulating a (stochastic) differential equation corresponding to the reverse-time process. Even with the introduction of their hybrid sampler, achieving high-fidelity results for high-resolution images still demands over 100 steps. Compared to the efficient samplers for diffusion models [40, 28, 29], which require around 10 steps to generate reasonable samples, DDBMs are falling behind, urging the development of efficient variants.

In this work, we present diffusion bridge implicit models (DBIMs) for accelerated sampling of DDBMs, motivated by the prominent denoising diffusion implicit models (DDIMs) [40]. Firstly, we explore the continuous-time forward process of DDBMs on discretized timesteps which are exactly the sampling timesteps, revealing them to be Markovian diffusion bridges. We demonstrate that these bridges can be generalized to a series of non-Markovian processes controlled by a variance parameter, while maintaining identical marginal distributions and training objectives as DDBMs. Secondly, the induced reverse generative processes correspond to sampling procedures of varying levels of stochasticity, including deterministic ones akin to implicit probabilistic models [31]. Consequently, DBIMs can be viewed as a bridge counterpart of DDIMs. Furthermore, by linking DBIMs to ordinary differential equations (ODEs), we discover that DBIMs can exactly yield the probability flow ODE (PF-ODE) in DDBMs without relying on advanced knowledge of differential equations such as the Fokker-Planck equation. Meanwhile, DBIMs prove to be significantly more efficient than simulating the PF-ODE as in DDBMs.

We demonstrate the superiority of DBIMs by applying them in image translation and restoration tasks, where they offer up to $25 \times$ faster sampling compared to DDBMs without extra training. Unlike conventional diffusion sampling, the initial step in DBIMs is forced to be stochastic with a booting noise to avoid singularity issues arising from the fixed starting point on a bridge. By viewing the booting noise as the latent variable, DBIMs maintain the generation diversity of typical generative models while enabling faithful encoding, reconstruction, and semantically meaningful interpolation in the data space.

2 Background

2.1 Diffusion Models

Given a d -dimensional data distribution $q_0(\mathbf{x}_0)$, diffusion models [44, 38, 16] build a diffusion process by defining a forward stochastic differential equation (SDE) starting from $\mathbf{x}_0 \sim q_0$:

$$d\mathbf{x}_t = f(t)\mathbf{x}_t dt + g(t)d\mathbf{w}_t \quad (1)$$

where $t \in [0, T]$ for some finite horizon T , $f, g : [0, T] \rightarrow \mathbb{R}$ is the scalar-valued drift and diffusion term, and $\mathbf{w}_t \in \mathbb{R}^d$ is a standard Wiener process. As a linear SDE, the forward process owns an analytic Gaussian transition kernel

$$q_{0t}(\mathbf{x}_t | \mathbf{x}_0) = \mathcal{N}(\alpha_t \mathbf{x}_0, \sigma_t^2 \mathbf{I}) \quad (2)$$

by Itô's formula [20], where α_t, σ_t are called *noise schedules* satisfying $f(t) = \frac{d \log \alpha_t}{dt}$, $g^2(t) = \frac{d\sigma_t^2}{dt} - 2\frac{d \log \alpha_t}{dt} \sigma_t^2$ [24]. The forward SDE is accompanied by a series of marginal distributions $\{q_t\}_{t=0}^T$ of $\{\mathbf{x}_t\}_{t=0}^T$, and f, g are properly designed so that the terminal distribution is approximately a pure Gaussian, i.e., $q_T(\mathbf{x}_T) \approx \mathcal{N}(\mathbf{0}, \sigma_T^2 \mathbf{I})$.

To sample from the data distribution $q_0(\mathbf{x}_0)$, we can solve the reverse SDE or probability flow ODE [44] from $t = T$ to $t = 0$:

$$d\mathbf{x}_t = [f(t)\mathbf{x}_t - g^2(t)\nabla_{\mathbf{x}_t} \log q_t(\mathbf{x}_t)]dt + g(t)d\bar{\mathbf{w}}_t, \quad (3)$$

$$d\mathbf{x}_t = \left[f(t)\mathbf{x}_t - \frac{1}{2}g^2(t)\nabla_{\mathbf{x}_t} \log q_t(\mathbf{x}_t) \right] dt. \quad (4)$$

They share the same marginal distributions $\{q_t\}_{t=0}^T$ with the forward SDE, where $\bar{\mathbf{w}}_t$ is the reverse-time Wiener process, and the only unknown term $\nabla_{\mathbf{x}_t} \log q_t(\mathbf{x}_t)$ is the *score function* of the marginal density q_t . By denoising score matching (DSM) [47], a score prediction network $\mathbf{s}_\theta(\mathbf{x}_t, t)$ can be parameterized to minimize $\mathbb{E}_t \mathbb{E}_{\mathbf{x}_0 \sim q_0(\mathbf{x}_0)} \mathbb{E}_{\mathbf{x}_t \sim q_{0t}(\mathbf{x}_t | \mathbf{x}_0)} [w(t) \|\mathbf{s}_\theta(\mathbf{x}_t, t) - \nabla_{\mathbf{x}_t} \log q_{0t}(\mathbf{x}_t | \mathbf{x}_0)\|_2^2]$, where q_{0t} is the analytic forward transition kernel and $w(t)$ is a positive weighting function. \mathbf{s}_θ can be plugged into the reverse SDE and the probability flow ODE to obtain the parameterized diffusion SDE and diffusion ODE. There are various dedicated solvers for diffusion SDE or ODE [40, 28, 29, 12, 51].

2.2 Denoising Diffusion Bridge Models

Denoising diffusion bridge models (DDBMs) [53] consider driving the diffusion process in Eqn. (1) to arrive at a particular point $\mathbf{y} \in \mathbb{R}^d$ almost surely via Doob's h -transform [11]:

$$d\mathbf{x}_t = f(t)\mathbf{x}_t dt + g^2(t)\nabla_{\mathbf{x}_t} \log q(\mathbf{x}_T = \mathbf{y} | \mathbf{x}_t) + g(t)d\mathbf{w}_t, \quad \mathbf{x}_0 \sim q_0 = p_{\text{data}}, \mathbf{x}_T = \mathbf{y}. \quad (5)$$

The endpoint \mathbf{y} is not restricted to Gaussian noise as in diffusion models, but instead chosen as informative priors (such as the degraded image in image restoration tasks). Given a starting point \mathbf{x}_0 , the process in Eqn. (5) also owns an analytic forward transition kernel

$$q(\mathbf{x}_t | \mathbf{x}_0, \mathbf{x}_T) = \mathcal{N}(a_t \mathbf{x}_T + b_t \mathbf{x}_0, c_t^2 \mathbf{I}), \quad a_t = \frac{\alpha_t}{\alpha_T} \frac{\text{SNR}_T}{\text{SNR}_t}, b_t = \alpha_t \left(1 - \frac{\text{SNR}_T}{\text{SNR}_t}\right), c_t^2 = \sigma_t^2 \left(1 - \frac{\text{SNR}_T}{\text{SNR}_t}\right) \quad (6)$$

which forms a *diffusion bridge*, and $\text{SNR}_t = \alpha_t^2 / \sigma_t^2$ is the signal-to-noise ratio at time t . DDBMs show that the forward process Eqn. (5) is associated with a reverse SDE and a probability flow ODE starting from $\mathbf{x}_T = \mathbf{y}$:

$$d\mathbf{x}_t = [f(t)\mathbf{x}_t - g^2(t)(\nabla_{\mathbf{x}_t} \log q(\mathbf{x}_t | \mathbf{x}_T = \mathbf{y}) - \nabla_{\mathbf{x}_t} \log q_{tT}(\mathbf{x}_T = \mathbf{y} | \mathbf{x}_t))] dt + g(t)d\mathbf{w}_t, \quad (7)$$

$$d\mathbf{x}_t = \left[f(t)\mathbf{x}_t - g^2(t) \left(\frac{1}{2} \nabla_{\mathbf{x}_t} \log q(\mathbf{x}_t | \mathbf{x}_T = \mathbf{y}) - \nabla_{\mathbf{x}_t} \log q_{tT}(\mathbf{x}_T = \mathbf{y} | \mathbf{x}_t) \right) \right] dt. \quad (8)$$

They share the same marginal distributions $\{q(\mathbf{x}_t | \mathbf{x}_T = \mathbf{y})\}_{t=0}^T$ with the forward process, where $\bar{\mathbf{w}}_t$ is the reverse-time Wiener process, q_{tT} is analytically known similar to Eqn. (2), and the only unknown term $\nabla_{\mathbf{x}_t} \log q(\mathbf{x}_t | \mathbf{x}_T = \mathbf{y})$ is the *bridge score function*. Denoising bridge score matching (DBSM) is proposed to learn the unknown score term $q(\mathbf{x}_t | \mathbf{x}_T = \mathbf{y})$ with a parameterized network $\mathbf{s}_\theta(\mathbf{x}_t, t, \mathbf{y})$, by minimizing

$$\mathcal{L}_w(\theta) = \mathbb{E}_t \mathbb{E}_{(\mathbf{x}_0, \mathbf{y}) \sim p_{\text{data}}(\mathbf{x}_0, \mathbf{y})} \mathbb{E}_{\mathbf{x}_t \sim q(\mathbf{x}_t | \mathbf{x}_0, \mathbf{x}_T = \mathbf{y})} [w(t) \|\mathbf{s}_\theta(\mathbf{x}_t, t, \mathbf{y}) - \nabla_{\mathbf{x}_t} \log q(\mathbf{x}_t | \mathbf{x}_0, \mathbf{x}_T = \mathbf{y})\|_2^2] \quad (9)$$

where $q(\mathbf{x}_t | \mathbf{x}_0, \mathbf{x}_T = \mathbf{y})$ is the forward transition kernel in Eqn. (6) and $w(t)$ is a positive weighting function. To sample from diffusion bridges with Eqn. (7) and Eqn. (8), DDBMs propose a high-order hybrid sampler that alternately simulates the ODE and SDE steps to enhance the sample quality, inspired by the Heun sampler in diffusion models [21]. However, the hybrid sampler is not dedicated to diffusion bridges, and lacks theoretical insights for developing efficient diffusion samplers.

3 Generative Model through Non-Markovian Diffusion Bridges

We start by examining the forward process of the diffusion bridge (Eqn. (5)) on a set of discretized timesteps $0 = t_0 < t_1 < \dots < t_{N-1} < t_N = T$, which will later serve as the timesteps for

sampling and can be chosen freely. We note that since the bridge score $\nabla_{\mathbf{x}_t} \log q(\mathbf{x}_t | \mathbf{x}_T)$ only depends on the marginal distribution $q(\mathbf{x}_t | \mathbf{x}_T)$, we can construct alternative probabilistic models while reusing the learned bridge score $\mathbf{s}_\theta(\mathbf{x}_t, t, \mathbf{x}_T)$, as long as they agree on the N marginal distributions $\{q(\mathbf{x}_{t_n} | \mathbf{x}_T)\}_{n=0}^{N-1}$. Besides, the new probabilistic models are defined on the discretized timesteps and induce new sampling procedures.

3.1 Non-Markovian Diffusion Bridges as Forward Process

We consider a family of probability distributions $q^{(\rho)}(\mathbf{x}_{t_0:N-1} | \mathbf{x}_T)$, controlled by a variance parameter $\rho \in \mathbb{R}^{N-1}$:

$$q^{(\rho)}(\mathbf{x}_{t_0:N-1} | \mathbf{x}_T) = q_0(\mathbf{x}_{t_0}) \prod_{n=1}^{N-1} q^{(\rho)}(\mathbf{x}_{t_n} | \mathbf{x}_0, \mathbf{x}_{t_{n+1}}, \mathbf{x}_T) \quad (10)$$

where q_0 is the data distribution at time 0 and for $1 \leq n \leq N-1$

$$q^{(\rho)}(\mathbf{x}_{t_n} | \mathbf{x}_0, \mathbf{x}_{t_{n+1}}, \mathbf{x}_T) = \mathcal{N}\left(a_{t_n} \mathbf{x}_T + b_{t_n} \mathbf{x}_0 + \sqrt{\frac{c_{t_n}^2 - \rho_n^2}{c_{t_{n+1}}}} \frac{\mathbf{x}_{t_{n+1}} - a_{t_{n+1}} \mathbf{x}_T - b_{t_{n+1}} \mathbf{x}_0}{c_{t_{n+1}}}, \rho_n^2 \mathbf{I}\right) \quad (11)$$

where ρ_n is the n -th element of ρ satisfying $\rho_{N-1} = c_{t_{N-1}}$. In the above expression, we reuse the notations of a_t, b_t, c_t in Eqn. (6), which are known coefficients determined by the diffusion noise schedule. Under this construction, we can prove that $q^{(\rho)}$ maintains consistency in marginal distributions with q defined in the forward process Eqn. (5).

Proposition 3.1 (Marginal Preservation, proof in Appendix B.1). *For $0 \leq n \leq N-1$, we have $q^{(\rho)}(\mathbf{x}_{t_n} | \mathbf{x}_T) = q(\mathbf{x}_{t_n} | \mathbf{x}_T)$.*

The definition of $q^{(\rho)}$ in Eqn. (10) represents the inference process, since it is factorized as the distribution of \mathbf{x}_{t_n} given $\mathbf{x}_{t_{n+1}}$ at the previous timestep. Such a representation facilitates the sampling process, which will we talk about later. Conversely, the forward process of $q^{(\rho)}$ can be induced by Bayes' rule as

$$q^{(\rho)}(\mathbf{x}_{t_{n+1}} | \mathbf{x}_0, \mathbf{x}_{t_n}, \mathbf{x}_T) = \frac{q^{(\rho)}(\mathbf{x}_{t_n} | \mathbf{x}_0, \mathbf{x}_{t_{n+1}}, \mathbf{x}_T) q^{(\rho)}(\mathbf{x}_{t_{n+1}} | \mathbf{x}_0, \mathbf{x}_T)}{q^{(\rho)}(\mathbf{x}_{t_n} | \mathbf{x}_0, \mathbf{x}_T)} \quad (12)$$

where $q^{(\rho)}(\mathbf{x}_t | \mathbf{x}_0, \mathbf{x}_T) = q(\mathbf{x}_t | \mathbf{x}_0, \mathbf{x}_T)$ is the marginal distribution of the diffusion bridge in Eqn. (6). As $\mathbf{x}_{t_{n+1}}$ in $q^{(\rho)}$ can simultaneously depend on \mathbf{x}_{t_n} and \mathbf{x}_0 , we refer to it as *non-Markovian diffusion bridges*, in contrast to Markovian bridges (such as Brownian bridges, and the diffusion bridge defined by the forward SDE in Eqn. (5)) which should satisfy $q(\mathbf{x}_{t_{n+1}} | \mathbf{x}_0, \mathbf{x}_{t_n}, \mathbf{x}_T) = q(\mathbf{x}_{t_{n+1}} | \mathbf{x}_{t_n}, \mathbf{x}_T)$.

3.2 Reverse Generative Process and Equivalent Training Objective

Since $q^{(\rho)}$ is defined by Eqn. (10) from an inference perspective, it can be naturally transformed into a parameterized and learnable generative model, by replacing the unknown \mathbf{x}_0 in Eqn. (10) with a *data predictor* $\mathbf{x}_\theta(\mathbf{x}_t, t, \mathbf{x}_T)$. Intuitively, \mathbf{x}_t on the diffusion bridge is a weighted mixture of $\mathbf{x}_T, \mathbf{x}_0$ and some random Gaussian noise according to Eqn. (6), where the weightings a_t, b_t, c_t are determined by the timestep t . The network \mathbf{x}_θ should be trained to recover the clean data \mathbf{x}_0 given $\mathbf{x}_t, \mathbf{x}_T$ and t .

Specifically, we define the generative process starting from \mathbf{x}_T as

$$p_\theta(\mathbf{x}_{t_n} | \mathbf{x}_{t_{n+1}}, \mathbf{x}_T) = \begin{cases} \mathcal{N}(\mathbf{x}_\theta(\mathbf{x}_{t_1}, t_1, \mathbf{x}_T), \rho_0^2 \mathbf{I}), & n = 0 \\ q^{(\rho)}(\mathbf{x}_{t_n} | \mathbf{x}_\theta(\mathbf{x}_{t_{n+1}}, t_{n+1}, \mathbf{x}_T), \mathbf{x}_{t_{n+1}}, \mathbf{x}_T), & 1 \leq n \leq N-1 \end{cases} \quad (13)$$

and the joint distribution as

$$p_\theta(\mathbf{x}_{t_0:N-1} | \mathbf{x}_T) = \prod_{n=0}^{N-1} p_\theta(\mathbf{x}_{t_n} | \mathbf{x}_{t_{n+1}}, \mathbf{x}_T) \quad (14)$$

To optimize the network parameter θ , we adopt the common variational inference objective as in DDPMs [16], except that the distributions are conditioned on \mathbf{x}_T :

$$\mathcal{J}^{(\rho)}(\theta) = \mathbb{E}_{q(\mathbf{x}_T)} \mathbb{E}_{q^{(\rho)}(\mathbf{x}_{t_0:N-1} | \mathbf{x}_T)} \left[\log q^{(\rho)}(\mathbf{x}_{t_1:N-1} | \mathbf{x}_0, \mathbf{x}_T) - \log p_\theta(\mathbf{x}_{t_0:N-1} | \mathbf{x}_T) \right] \quad (15)$$

where $q^{(\rho)}$ and p_θ are defined in Eqn. (10) and Eqn. (14) respectively. It seems that the objective \mathcal{L}_w in Eqn. (9) is distinct from $\mathcal{J}^{(\rho)}$: Respectively, they are defined on continuous and discrete timesteps; they originate from score matching and variational inference; they have different parameterizations of score and data prediction². However, we show that they are equivalent by focusing on the discretized timesteps and transforming the parameterization.

Proposition 3.2 (Training Equivalence, proof in Appendix B.2). *For $\rho > \mathbf{0}$, there exists certain weights γ so that $\mathcal{J}^{(\rho)}(\theta) = \mathcal{L}_\gamma(\theta) + C$ on the discretized timesteps $\{t_n\}_{n=1}^N$, where C is a constant irrelevant to θ . Besides, the bridge score predictor s_θ in $\mathcal{L}_\gamma(\theta)$ has the following relationship with the data predictor x_θ in $\mathcal{J}^{(\rho)}(\theta)$:*

$$s_\theta(\mathbf{x}_t, t, \mathbf{x}_T) = -\frac{\mathbf{x}_t - a_t \mathbf{x}_T - b_t \mathbf{x}_\theta(\mathbf{x}_t, t, \mathbf{x}_T)}{c_t^2} \quad (16)$$

Though the weighting γ may not precisely match the actually weighting w used in training s_θ , this discrepancy doesn't affect our utilization of s_θ . On the one hand, \mathcal{L} consists of independent terms concerning individual timesteps (as long as the network's parameters are not shared across different t), ensuring that the global minimum remains the same as minimizing the loss at each timestep, regardless of the weighting. On the other hand, \mathcal{L} under different weightings are mutually bounded by $\frac{\min_t w_t}{\max_t \gamma_t} \mathcal{L}_\gamma(\theta) \leq \mathcal{L}_w(\theta) \leq \frac{\max_t w_t}{\min_t \gamma_t} \mathcal{L}_\gamma(\theta)$. Besides, it is widely acknowledged that in diffusion models, the weighting corresponding to variational inference may yield superior likelihood but suboptimal sample quality [16, 44], which is not preferred in practice. Hence, it is reasonable to reuse the network trained by \mathcal{L} under other weightings while leveraging various ρ for improved sample efficiency.

4 Sampling with Generalized Diffusion Bridges

Now that we have confirmed the rationality and built the theoretical foundations for applying the generalized diffusion bridge p_θ (Eqn. (14)) to pretrained DDBMs, a range of inference processes is now at our disposal, controlled by the variance parameter ρ . This positions us to explore the resultant sampling procedures and the effects of ρ in pursuit of better and more efficient generation.

4.1 Diffusion Bridge Implicit Models

Suppose we sample in reverse time on the discretized timesteps $0 = t_0 < t_1 < \dots < t_{N-1} < t_N = T$. The number N and the schedule of sampling steps can be made independently of the original timesteps on which the bridge model is trained, whether discrete [25] or continuous [53]. According to the generative process of p_θ in Eqn. (13), the updating rule from t_{n+1} to t_n is described by

$$\mathbf{x}_{t_n} = a_{t_n} \mathbf{x}_T + b_{t_n} \hat{\mathbf{x}}_0 + \underbrace{\sqrt{c_{t_n}^2 - \rho_n^2} \frac{\mathbf{x}_{t_{n+1}} - a_{t_{n+1}} \mathbf{x}_T - b_{t_{n+1}} \hat{\mathbf{x}}_0}{c_{t_{n+1}}}}_{\text{predicted noise } \hat{\epsilon}} + \rho_n \epsilon, \quad \epsilon \sim \mathcal{N}(\mathbf{0}, \mathbf{I}) \quad (17)$$

where $\hat{\mathbf{x}}_0 = \mathbf{x}_\theta(\mathbf{x}_{t_{n+1}}, t_{n+1}, \mathbf{x}_T)$ denotes the predicted clean data at time 0.

Intuition of the Sampling Procedure Intuitively, the form of Eqn. (17) bears a resemblance to the forward transition kernel of the diffusion bridge in Eqn. (6) (which can be rewritten as $\mathbf{x}_t = a_t \mathbf{x}_T + b_t \mathbf{x}_0 + c_t \epsilon$, $\epsilon \sim \mathcal{N}(\mathbf{0}, \mathbf{I})$). Compared to the forward process, \mathbf{x}_0 is substituted with the predicted $\hat{\mathbf{x}}_0$, and a portion of the standard Gaussian noise ϵ now stems from the predicted noise $\hat{\epsilon}$. The predicted noise $\hat{\epsilon}$ is derived from $\mathbf{x}_{t_{n+1}}$ at the previous timestep and can be expressed by the predicted clean data $\hat{\mathbf{x}}_0$.

We investigate the effects of the variance parameter ρ from the theoretical perspective by considering two extreme cases. Firstly, we note that when $\rho_n = \sigma_{t_n} \sqrt{1 - \frac{\text{SNR}_{t_{n+1}}}{\text{SNR}_{t_n}}}$ for each $0 \leq n \leq N - 1$, the \mathbf{x}_T term in Eqn. (17) is canceled out. In this scenario, the forward process in Eqn. (4.1) becomes a Markovian bridge (see details in Appendix C). Besides, the inference process will get rid of \mathbf{x}_T

²The diffusion bridge models are usually parameterized differently from score prediction, but can be converted to score prediction. See Appendix D.1 for details.

Table 1: Comparison between different diffusion models and diffusion bridge models.

	Diffusion Models			Diffusion Bridge Models	
	DDPM [16]	ScoreSDE [44]	DDIM [40]	DDBM [53]	DBIM (Ours)
Timesteps	Discrete	Continuous	Discrete	Continuous	Discrete
Forward Distribution	$q(\mathbf{x}_n \mathbf{x}_0)$	$q(\mathbf{x}_t \mathbf{x}_0)$	$q(\mathbf{x}_n \mathbf{x}_{n-1}, \mathbf{x}_0)$	$q(\mathbf{x}_t \mathbf{x}_0, \mathbf{x}_T)$	$q(\mathbf{x}_{t_{n+1}} \mathbf{x}_0, \mathbf{x}_{t_n}, \mathbf{x}_T)$
Inference Process	$p_\theta(\mathbf{x}_{n-1} \mathbf{x}_n)$	SDE/ODE	$p_\theta(\mathbf{x}_{n-1} \mathbf{x}_n)$	SDE/ODE	$p_\theta(\mathbf{x}_{t_n} \mathbf{x}_{t_{n+1}}, \mathbf{x}_T)$
Markovian	✓	✓	✗	✓	✗

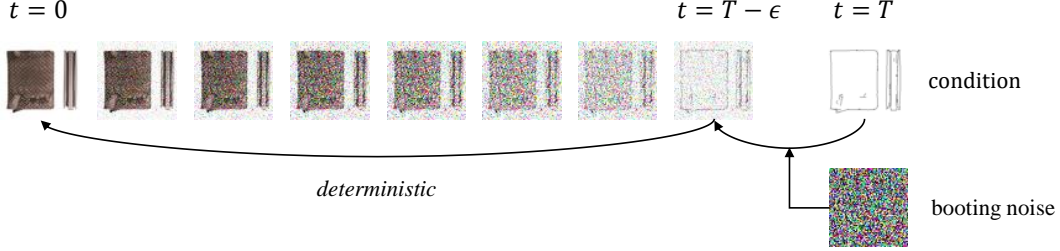


Figure 2: Illustration of the DBIM’s deterministic sampling procedure when $\rho = 0$.

and simplify to $p_\theta(\mathbf{x}_{t_n}|\mathbf{x}_{t_{n+1}})$, akin to the sampling mechanism in DDPMs [16]. Secondly, when $\rho_n = 0$ for each $0 \leq n \leq N - 1$, the inference process will be free from random noise and composed of deterministic iterative updates, characteristic of an implicit probabilistic model [31]. Consequently, we name the resulting model *diffusion bridge implicit models* (DBIMs), drawing parallels with denoising diffusion implicit models (DDIMs) [40], a widely adopted technique to expedite the sampling of diffusion models. DBIMs serve as the bridge counterpart and extension of DDIMs, as illustrated in Table 1.

When we choose ρ that lies between these two boundary cases, we can obtain non-Markovian diffusion bridges with intermediate and non-zero stochastic levels. Such bridges may potentially yield superior sample quality. We present detailed ablations in Section 5.1.

The Singularity at the Initial Step for Deterministic Sampling One important aspect to note regarding DBIMs is that its initial step exhibits singularity when $\rho = 0$, a property essentially distinct from DDIMs in diffusion models. Specifically, in the initial step we have $t_{n+1} = T$, and $c_{t_{n+1}}$ in the denominator in Eqn. (17) equals 0. This phenomenon can be understood intuitively: given a fixed starting point \mathbf{x}_T , the variable \mathbf{x}_t for $t < T$ is typically still stochastically distributed (the marginal $p_\theta(\mathbf{x}_t|\mathbf{x}_T)$ is not a Dirac distribution). For instance, in inpainting tasks, there should be various plausible complete images corresponding to a fixed masked image. However, a fully deterministic sampling procedure disrupts such stochasticity.

To tackle this, we are forced to employ the other boundary choice $\rho_n = \sigma_{t_n} \sqrt{1 - \frac{\text{SNR}_{t_{n+1}}}{\text{SNR}_{t_n}}}$ in the initial step³, which is aligned with our previous restriction that $\rho_{N-1} = c_{t_{N-1}}$. This will introduce an additional standard Gaussian noise ϵ which we term as the *booting noise*. It accounts for the stochasticity of the final sample \mathbf{x}_0 under a given fixed \mathbf{x}_T and can be viewed as the latent variable. We illustrate the complete DBIM pipeline in Figure 2.

4.2 Connection to Probability Flow ODE

It is intuitive to perceive that the deterministic sampling can be related to solving an ODE. By setting $\rho = 0, t_{n+1} = t$ and $t_{n+1} - t_n = \Delta t$ in Eqn. (17), the DBIM updating rule can be reorganized as

$$\frac{\mathbf{x}_{t-\Delta t}}{c_{t-\Delta t}} = \frac{\mathbf{x}_t}{c_t} + \left(\frac{a_{t-\Delta t}}{c_{t-\Delta t}} - \frac{a_t}{c_t} \right) \mathbf{x}_T + \left(\frac{b_{t-\Delta t}}{c_{t-\Delta t}} - \frac{b_t}{c_t} \right) \mathbf{x}_\theta(\mathbf{x}_t, t, \mathbf{x}_T) \quad (18)$$

As a_t, b_t, c_t are continuous functions of time t defined in Eqn. (6), the ratios $\frac{a_t}{c_t}$ and $\frac{b_t}{c_t}$ also remain continuous functions of t . Therefore, Eqn. (18) can be treated as an Euler discretization of the

³With this choice, $c_{t_{n+1}}$ in the denominator in Eqn. (17) will be canceled out.

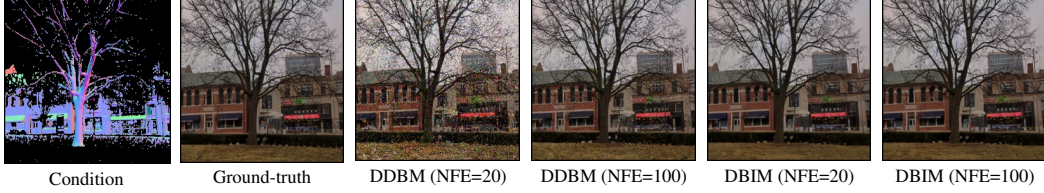


Figure 3: Image translation results on the DIODE-Outdoor dataset with DDBM and DBIM.

following ordinary differential equation (ODE):

$$d \begin{pmatrix} \mathbf{x}_t \\ c_t \end{pmatrix} = \mathbf{x}_T d \begin{pmatrix} a_t \\ c_t \end{pmatrix} + \mathbf{x}_\theta(\mathbf{x}_t, t, \mathbf{x}_T) d \begin{pmatrix} b_t \\ c_t \end{pmatrix} \quad (19)$$

We retain this form due to its extreme neatness. Though it does not resemble a conventional ODE involving dt , the two infinitesimal terms $d \begin{pmatrix} a_t \\ c_t \end{pmatrix}$ and $d \begin{pmatrix} b_t \\ c_t \end{pmatrix}$ can indeed be expressed with dt by the chain rule of derivatives. The ODE form of DBIMs also suggests that with a sufficient number of discretization steps, we can reverse the sampling process and obtain encodings of the observed data, which can be useful for interpolation or other downstream tasks.

In DDBMs, a probability flow ODE (PF-ODE, Eqn. (8)) involving $d\mathbf{x}_t$ and dt is proposed and used for deterministic sampling. We reveal in the following proposition that our ODE in Eqn. (19) can exactly yield the PF-ODE, while the derivation of our ODE does not rely on any advanced knowledge of differential equations (such as the Fokker-Planck equation), but pure probabilistic models.

Proposition 4.1 (Equivalence to Probability Flow ODE, proof in Appendix B.3). *Suppose $s_\theta(\mathbf{x}_t, t, \mathbf{x}_T)$ is learned as the ground-truth bridge score $\nabla_{\mathbf{x}_t} \log q(\mathbf{x}_t | \mathbf{x}_T)$, and \mathbf{x}_θ is related to s_θ through Eqn. (16), then Eqn. (19) can be converted to the probability flow ODE (Eqn. (8)) proposed in DDBMs.*

Though the conversion from our ODE to the PF-ODE is straightforward, the reverse conversion can be non-trivial and may require utilizing more advanced tools such as exponential integrators [4, 18]. Despite their theoretical equivalence, our ODE describes the evolution of $\frac{\mathbf{x}_t}{c_t}$ rather than \mathbf{x}_t , and its discretization is performed with respect to $d \begin{pmatrix} a_t \\ c_t \end{pmatrix}$ and $d \begin{pmatrix} b_t \\ c_t \end{pmatrix}$ instead of dt . Empirically, DBIMs prove significantly more efficient than the Euler discretization of the PF-ODE, thereby accelerating DDBMs by a substantial margin.

5 Experiments

In this section, we show that DBIMs surpass the original sampling procedure of DDBMs by a large margin, in terms of both sample quality and sample efficiency. We also showcase DBIM’s capabilities in latent-space encoding, reconstruction, and interpolation using deterministic sampling. All comparisons between DBIMs and DDBMs are conducted using identically trained models. For DDBMs, we employ their proposed hybrid sampler for sampling. For DBIMs, we control the variance parameter ρ by interpolating between its boundary selections:

$$\rho_n = \eta \sigma_{t_n} \sqrt{1 - \frac{\text{SNR}_{t_{n+1}}}{\text{SNR}_{t_n}}}, \quad \eta \in [0, 1] \quad (20)$$

where $\eta = 0$ corresponds to deterministic sampling and $\eta = 1$ corresponds to Markovian stochastic sampling. Note that while in diffusion models, the Markovian case of DDIMs degrades to DDPMs (i.e., the original sampler for discrete-time diffusion models), DDBMs are initially defined over continuous time and sampled by simulating differential equations. Consequently, DBIMs with $\eta = 1$ also serve as a novel sampling scheme for DDBMs.

We conduct experiments including (1) image-to-image translation tasks on Edges→Handbags [19] (64×64) and DIODE-Outdoor [46] (256×256) (2) image restoration task of inpainting on ImageNet [9] (256×256) with 128×128 center mask. We report the Fréchet inception distance (FID) [14] for all experiments, and additionally measure Inception Scores (IS) [2], Learned Perceptual Image Patch Similarity (LPIPS) [50], Mean Square Error (MSE) (for image-to-image translation)

Table 2: Quantitative results in the image translation task. [†]Baseline results are taken directly from DDBMs, where they did not report the exact NFE.

	NFE	Edges→Handbags (64 × 64)				DIODE-Outdoor (256 × 256)			
		FID ↓	IS ↑	LPIPS ↓	MSE ↓	FID ↓	IS ↑	LPIPS ↓	MSE ↓
Pix2Pix [19]	1	74.8	3.24	0.356	0.209	82.4	4.22	0.556	0.133
DDIB [45]	≥ 40 [†]	186.84	2.04	0.869	1.05	242.3	4.22	0.798	0.794
SDEdit [30]	≥ 40	26.5	3.58	0.271	0.510	31.14	5.70	0.714	0.534
Rectified Flow [26]	≥ 40	25.3	2.80	0.241	0.088	77.18	5.87	0.534	0.157
I ² SB [25]	≥ 40	7.43	3.40	0.244	0.191	9.34	5.77	0.373	0.145
DDBM [53]	118	1.83	3.73	0.142	0.040	4.43	6.21	0.244	0.084
DDBM [53]	200	0.88	3.69	0.110	0.006	3.34	5.95	0.215	0.020
DBIM (Ours)	20	1.74	3.64	0.095	0.005	4.99	6.10	0.201	0.017
DBIM (Ours)	100	0.89	3.62	0.100	0.006	2.57	6.06	0.198	0.018

Table 3: Quantative results in the image restoration task.

Inpainting	ImageNet (256 × 256)		
	NFE	FID ↓	CA ↑
<i>Center</i> (128 × 128)			
DDRM [22]	20	24.4	62.1
IIGDM [41]	100	7.3	72.6
DDNM [48]	100	15.1	55.9
Palette [35]	1000	6.1	63.0
I ² SB [25]	1000	4.9	66.1
DDBM [53]	500	4.27	71.8
DBIM (Ours)	20	4.17	72.2
DBIM (Ours)	100	3.88	72.6

Table 4: Ablation of the variance parameter controlled by η for image restoration, measured by FID.

Sampler	NFE						
	5	10	20	50	100	200	500
	Inpainting, ImageNet (256 × 256), <i>Center</i> (128 × 128)						
η	0.0	6.47	4.62	4.17	4.00	3.95	3.95
	0.3	6.61	4.66	4.19	4.02	3.99	3.99
	0.5	6.77	4.69	4.19	3.98	3.92	3.94
	0.8	7.33	4.97	4.21	3.91	3.88	3.86
	1.0	8.90	5.73	4.53	4.02	3.91	3.87
DDBM	275.25	57.18	29.65	10.63	6.46	4.95	4.27

and Classifier Accuracy (CA) (for image inpainting), following previous works [25, 53]. The metrics are computed using the complete training set for Edges→Handbags and DIODE-Outdoor, and 10,000 images from validation set for ImageNet. Additional experiment details are provided in Appendix D.

5.1 Sample Quality and Efficiency

We present the quantitative results of DBIMs in Table 2 and Table 3, compared with baselines including GAN-based, diffusion-based and bridge-based methods. We set the number of function evaluations (NFEs) of DBIM to 20 and 100 to demonstrate both efficiency at small NFEs and quality at large NFEs. We select η from the set [0.0, 0.3, 0.5, 0.8, 1.0] for DBIM and report the best results.

In image translation tasks, DDBM achieves the best sample quality (measured by FID) among the baselines, but requires NFE > 100. In contrast, DBIM with only NFE = 20 already surpasses all baselines, performing better than or on par with DDBM at NFE = 118. When increasing the NFE to 100, DBIM further improves the sample quality and outperforms DDBM with NFE = 200 on DIODE-Outdoor. In the more challenging image inpainting task on ImageNet 256 × 256, the superiority of DBIM is highlighted even further. In particular, DBIM with NFE = 20 outperforms all baselines, including DDBM with NFE = 500, achieving a 25× speed-up. With NFE = 100, DBIM continues to improve sample quality, reaching a FID lower than 4 for the first time.

The comparison of visual quality is illustrated in Figure 1 and Figure 3, where DBIM produces smoother outputs with significantly fewer noisy artifacts compared to DDBM’s hybrid sampler. Additional samples are provided in Appendix E.

Ablation of the Variance Parameter We investigate the impact of the variance parameter ρ (controlled by η) to identify how the level of stochasticity affects sample quality across various NFEs, as shown in Table 4 and Table 5. For image translation tasks, we consistently observe that employing a deterministic sampler with $\eta = 0.0$ yields superior performance compared to stochastic samplers with $\eta > 0$. We attribute it to the characteristics of the datasets, where the target image is highly correlated with and dependent on the condition, resulting in a generative model that lacks diversity. In this case, a straightforward mapping without the involvement of stochasticity is preferred. Conversely, for image inpainting on the more diverse dataset ImageNet 256 × 256, the parameter η exhibits significance across different NFEs. When NFE ≤ 20, $\eta = 0.0$ is the optimal choice, with FID steadily increasing as η ascends. However, when NFE ≥ 50, a relatively large level of stochasticity at $\eta = 0.8$ or even $\eta = 1.0$ yields optimal FID. Notably, the FID of $\eta = 0.0$ converges to 3.95 at NFE = 100,

Table 5: Ablation of the variance parameter controlled by η for image translation, measured by FID.

Sampler	NFE														
	5	10	20	50	100	200	500	5	10	20	50	100	200	500	
	Image Translation, Edges→Handbags (64×64)							Image Translation, DIODE-Outdoor (256×256)							
η	0.0	3.60	2.46	1.74	1.14	0.89	0.74	0.65	14.25	7.98	4.99	3.20	2.57	2.27	2.09
	0.3	3.70	2.63	1.93	1.26	0.99	0.85	0.74	14.44	8.18	5.12	3.31	2.69	2.33	2.13
	0.5	3.78	2.76	1.99	1.35	1.04	0.88	0.74	14.89	8.63	5.50	3.62	2.91	2.46	2.21
	0.8	3.97	3.08	2.20	1.64	1.22	1.01	0.80	16.34	10.17	6.85	4.57	3.56	2.93	2.46
	1.0	4.28	3.50	2.64	2.03	1.50	1.19	0.92	19.09	12.53	8.80	5.97	4.53	3.63	2.85
DDBM		317.22	137.15	46.74	7.79	2.40	0.88	0.53	328.33	151.93	41.03	15.19	6.54	3.34	2.26

with no further improvement at larger NFEs, indicating convergence to the ground-truth sample by the corresponding PF-ODE. This observation aligns with diffusion models, where deterministic sampling facilitates rapid convergence, while introducing stochasticity in sampling enhances diversity, ultimately culminating in the highest sample quality when NFE is substantial.

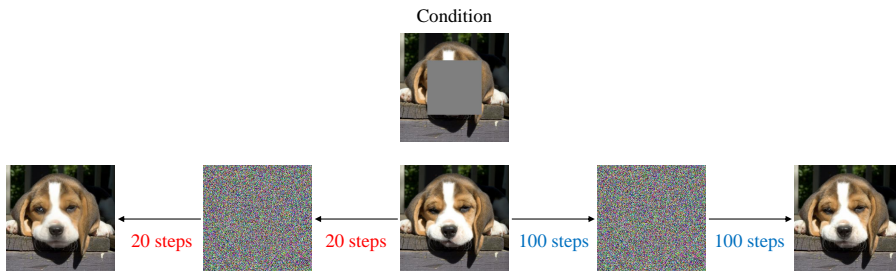


Figure 4: Encoding and reconstruction with deterministic DBIMs.



Figure 5: Semantic interpolation with deterministic DBIMs.

5.2 Reconstruction and Interpolation

As discussed in Section 4.2, the deterministic nature of DBIMs at $\eta = 0$ and its connection to neural ODEs enable faithful encoding and reconstruction by treating the booting noise as the latent variable. Furthermore, employing spherical linear interpolation in the latent space and subsequently decoding back to the image space allows for semantic image interpolation in image translation and image restoration tasks. These capabilities cannot be achieved by DBIMs with $\eta > 0$, or by DDBM’s hybrid sampler which incorporates stochastic steps. We showcase the encoding and decoding results in Figure 4, indicating that accurate reconstruction is achievable with a sufficient number of sampling steps. We also illustrate the interpolation process in Figure 5.

6 Conclusion

In this work, we introduce diffusion bridge implicit models (DBIMs) for accelerated sampling of DDBMs without extra training. In contrast to DDBM’s continuous-time generation processes, we concentrate on discretized sampling steps and propose a series of novel generative probabilistic models on them, spanning from Markovian to non-Markovian variants. The induced sampling procedures serve as bridge counterparts and extensions of DDIMs, filling the missing perspectives of diffusion bridges. Experiments on high-resolution datasets and challenging inpainting tasks demonstrate DBIM’s superiority in both the sample quality and sample efficiency, achieving state-of-the-art FID scores with 100 steps and providing up to $25\times$ acceleration of DDBM’s sampling procedure.

Limitations and broader impact Despite the notable speed-up for diffusion bridges, DIBMs still lag behind GAN-based methods in one-step generation, and are not fast enough for real-time applications. The efficiency of DBIMs can reduce computational resources and energy consumption in deploying diffusion bridge models. However, they may also facilitate the potential misuse for generating fake and malicious media content, and amplify undesirable social bias that could already exist in the training dataset.

Acknowledgements

This work was supported by the National Key Research and Development Program of China (No. 2021ZD0110502), NSFC Projects (Nos. 62061136001, 62106123, 62076147, U19A2081, 61972224, 62106120), Tsinghua Institute for Guo Qiang, and the High Performance Computing Center, Tsinghua University. J.Z is also supported by the XPlorer Prize.

References

- [1] Fan Bao, Chendong Xiang, Gang Yue, Guande He, Hongzhou Zhu, Kaiwen Zheng, Min Zhao, Shilong Liu, Yaole Wang, and Jun Zhu. Vidu: a highly consistent, dynamic and skilled text-to-video generator with diffusion models. *arXiv preprint arXiv:2405.04233*, 2024.
- [2] Shane Barratt and Rishi Sharma. A note on the inception score. *arXiv preprint arXiv:1801.01973*, 2018.
- [3] Christopher M Bishop and Nasser M Nasrabadi. *Pattern recognition and machine learning*, volume 4. Springer, 2006.
- [4] Mari Paz Calvo and César Palencia. A class of explicit multistep exponential integrators for semilinear problems. *Numerische Mathematik*, 102:367–381, 2006.
- [5] Nanxin Chen, Yu Zhang, Heiga Zen, Ron J. Weiss, Mohammad Norouzi, and William Chan. Wavegrad: Estimating gradients for waveform generation. In *International Conference on Learning Representations*, 2021.
- [6] Zehua Chen, Guande He, Kaiwen Zheng, Xu Tan, and Jun Zhu. Schrodinger bridges beat diffusion models on text-to-speech synthesis. *arXiv preprint arXiv:2312.03491*, 2023.
- [7] Hyungjin Chung, Jeongsol Kim, Michael Thompson Mccann, Marc Louis Klasky, and Jong Chul Ye. Diffusion posterior sampling for general noisy inverse problems. In *The Eleventh International Conference on Learning Representations*, 2022.
- [8] Valentin De Bortoli, James Thornton, Jeremy Heng, and Arnaud Doucet. Diffusion schrödinger bridge with applications to score-based generative modeling. *Advances in Neural Information Processing Systems*, 34:17695–17709, 2021.
- [9] Jia Deng, Wei Dong, Richard Socher, Li-Jia Li, Kai Li, and Li Fei-Fei. ImageNet: A large-scale hierarchical image database. In *2009 IEEE Conference on Computer Vision and Pattern Recognition*, pages 248–255. IEEE, 2009.
- [10] Prafulla Dhariwal and Alexander Quinn Nichol. Diffusion models beat GANs on image synthesis. In *Advances in Neural Information Processing Systems*, volume 34, pages 8780–8794, 2021.
- [11] Joseph L Doob and JI Doob. *Classical potential theory and its probabilistic counterpart*, volume 262. Springer, 1984.
- [12] Martin Gonzalez, Nelson Fernandez, Thuy Tran, Elies Gherbi, Hatem Hajri, and Nader Mas-moudi. Seeds: Exponential sde solvers for fast high-quality sampling from diffusion models. *arXiv preprint arXiv:2305.14267*, 2023.
- [13] Agrim Gupta, Lijun Yu, Kihyuk Sohn, Xiuye Gu, Meera Hahn, Li Fei-Fei, Irfan Essa, Lu Jiang, and José Lezama. Photorealistic video generation with diffusion models. *arXiv preprint arXiv:2312.06662*, 2023.

- [14] Martin Heusel, Hubert Ramsauer, Thomas Unterthiner, Bernhard Nessler, and Sepp Hochreiter. GANs trained by a two time-scale update rule converge to a local Nash equilibrium. In Isabelle Guyon, Ulrike von Luxburg, Samy Bengio, Hanna M. Wallach, Rob Fergus, S. V. N. Vishwanathan, and Roman Garnett, editors, *Advances in Neural Information Processing Systems*, volume 30, pages 6626–6637, 2017.
- [15] Jonathan Ho, William Chan, Chitwan Saharia, Jay Whang, Ruiqi Gao, Alexey Gritsenko, Diederik P Kingma, Ben Poole, Mohammad Norouzi, David J Fleet, et al. Imagen video: High definition video generation with diffusion models. *arXiv preprint arXiv:2210.02303*, 2022.
- [16] Jonathan Ho, Ajay Jain, and Pieter Abbeel. Denoising diffusion probabilistic models. In *Advances in Neural Information Processing Systems*, volume 33, pages 6840–6851, 2020.
- [17] Jonathan Ho and Tim Salimans. Classifier-free diffusion guidance. In *NeurIPS 2021 Workshop on Deep Generative Models and Downstream Applications*, 2021.
- [18] Marlis Hochbruck, Alexander Ostermann, and Julia Schweitzer. Exponential rosenbrock-type methods. *SIAM Journal on Numerical Analysis*, 47(1):786–803, 2009.
- [19] Phillip Isola, Jun-Yan Zhu, Tinghui Zhou, and Alexei A Efros. Image-to-image translation with conditional adversarial networks. In *Proceedings of the IEEE conference on computer vision and pattern recognition*, pages 1125–1134, 2017.
- [20] Kiyosi Itô. On a formula concerning stochastic differentials. *Nagoya Mathematical Journal*, 3:55–65, 1951.
- [21] Tero Karras, Miika Aittala, Timo Aila, and Samuli Laine. Elucidating the design space of diffusion-based generative models. In *Advances in Neural Information Processing Systems*, 2022.
- [22] Bahjat Kawar, Michael Elad, Stefano Ermon, and Jiaming Song. Denoising diffusion restoration models. In *Advances in Neural Information Processing Systems*, 2022.
- [23] Dongjun Kim, Chieh-Hsin Lai, Wei-Hsiang Liao, Naoki Murata, Yuhta Takida, Toshimitsu Uesaka, Yutong He, Yuki Mitsufuji, and Stefano Ermon. Consistency trajectory models: Learning probability flow ode trajectory of diffusion. In *The Twelfth International Conference on Learning Representations*, 2023.
- [24] Diederik P Kingma, Tim Salimans, Ben Poole, and Jonathan Ho. Variational diffusion models. In *Advances in Neural Information Processing Systems*, 2021.
- [25] Guan-Horng Liu, Arash Vahdat, De-An Huang, Evangelos Theodorou, Weili Nie, and Anima Anandkumar. I²sb: Image-to-image schrödinger bridge. In *International Conference on Machine Learning*, pages 22042–22062. PMLR, 2023.
- [26] Xingchao Liu, Chengyue Gong, et al. Flow straight and fast: Learning to generate and transfer data with rectified flow. In *The Eleventh International Conference on Learning Representations*, 2022.
- [27] Cheng Lu, Kaiwen Zheng, Fan Bao, Jianfei Chen, Chongxuan Li, and Jun Zhu. Maximum likelihood training for score-based diffusion odes by high order denoising score matching. In *International Conference on Machine Learning*, pages 14429–14460. PMLR, 2022.
- [28] Cheng Lu, Yuhao Zhou, Fan Bao, Jianfei Chen, Chongxuan Li, and Jun Zhu. Dpm-solver: A fast ode solver for diffusion probabilistic model sampling in around 10 steps. In *Advances in Neural Information Processing Systems*, 2022.
- [29] Cheng Lu, Yuhao Zhou, Fan Bao, Jianfei Chen, Chongxuan Li, and Jun Zhu. Dpm-solver++: Fast solver for guided sampling of diffusion probabilistic models. *arXiv preprint arXiv:2211.01095*, 2022.
- [30] Chenlin Meng, Yang Song, Jiaming Song, Jiajun Wu, Jun-Yan Zhu, and Stefano Ermon. SDEdit: Image synthesis and editing with stochastic differential equations. In *International Conference on Learning Representations*, 2022.

- [31] Shakir Mohamed and Balaji Lakshminarayanan. Learning in implicit generative models. *arXiv preprint arXiv:1610.03483*, 2016.
- [32] Alexander Quinn Nichol, Prafulla Dhariwal, Aditya Ramesh, Pranav Shyam, Pamela Mishkin, Bob McGrew, Ilya Sutskever, and Mark Chen. Glide: Towards photorealistic image generation and editing with text-guided diffusion models. In *International Conference on Machine Learning*, pages 16784–16804. PMLR, 2022.
- [33] Aditya Ramesh, Prafulla Dhariwal, Alex Nichol, Casey Chu, and Mark Chen. Hierarchical text-conditional image generation with CLIP latents. *arXiv preprint arXiv:2204.06125*, 2022.
- [34] Robin Rombach, Andreas Blattmann, Dominik Lorenz, Patrick Esser, and Björn Ommer. High-resolution image synthesis with latent diffusion models. In *Proceedings of the IEEE/CVF Conference on Computer Vision and Pattern Recognition*, pages 10684–10695, 2022.
- [35] Chitwan Saharia, William Chan, Huiwen Chang, Chris Lee, Jonathan Ho, Tim Salimans, David Fleet, and Mohammad Norouzi. Palette: Image-to-image diffusion models. In *ACM SIGGRAPH 2022 Conference Proceedings*, pages 1–10, 2022.
- [36] Axel Sauer, Dominik Lorenz, Andreas Blattmann, and Robin Rombach. Adversarial diffusion distillation. *arXiv preprint arXiv:2311.17042*, 2023.
- [37] Yuyang Shi, Valentin De Bortoli, Andrew Campbell, and Arnaud Doucet. Diffusion schrödinger bridge matching. *Advances in Neural Information Processing Systems*, 36, 2024.
- [38] Jascha Sohl-Dickstein, Eric Weiss, Niru Maheswaranathan, and Surya Ganguli. Deep unsupervised learning using nonequilibrium thermodynamics. In *International Conference on Machine Learning*, pages 2256–2265. PMLR, 2015.
- [39] Vignesh Ram Somnath, Matteo Pariset, Ya-Ping Hsieh, Maria Rodriguez Martinez, Andreas Krause, and Charlotte Bunne. Aligned diffusion schrödinger bridges. In *Uncertainty in Artificial Intelligence*, pages 1985–1995. PMLR, 2023.
- [40] Jiaming Song, Chenlin Meng, and Stefano Ermon. Denoising diffusion implicit models. In *International Conference on Learning Representations*, 2021.
- [41] Jiaming Song, Arash Vahdat, Morteza Mardani, and Jan Kautz. Pseudoinverse-guided diffusion models for inverse problems. In *International Conference on Learning Representations*, 2023.
- [42] Yang Song, Prafulla Dhariwal, Mark Chen, and Ilya Sutskever. Consistency models. In *International Conference on Machine Learning*, pages 32211–32252. PMLR, 2023.
- [43] Yang Song, Conor Durkan, Iain Murray, and Stefano Ermon. Maximum likelihood training of score-based diffusion models. In *Advances in Neural Information Processing Systems*, volume 34, pages 1415–1428, 2021.
- [44] Yang Song, Jascha Sohl-Dickstein, Diederik P. Kingma, Abhishek Kumar, Stefano Ermon, and Ben Poole. Score-based generative modeling through stochastic differential equations. In *International Conference on Learning Representations*, 2021.
- [45] Xuan Su, Jiaming Song, Chenlin Meng, and Stefano Ermon. Dual diffusion implicit bridges for image-to-image translation. *arXiv preprint arXiv:2203.08382*, 2022.
- [46] Igor Vasiljevic, Nick Kolkin, Shanyi Zhang, Ruotian Luo, Haochen Wang, Falcon Z Dai, Andrea F Daniele, Mohammadreza Mostajabi, Steven Basart, Matthew R Walter, et al. Diode: A dense indoor and outdoor depth dataset. *arXiv preprint arXiv:1908.00463*, 2019.
- [47] Pascal Vincent. A connection between score matching and denoising autoencoders. *Neural computation*, 23(7):1661–1674, 2011.
- [48] Yinhuai Wang, Jiwen Yu, and Jian Zhang. Zero-shot image restoration using denoising diffusion null-space model. In *The Eleventh International Conference on Learning Representations*, 2023.

- [49] Qinsheng Zhang and Yongxin Chen. Fast sampling of diffusion models with exponential integrator. In *The Eleventh International Conference on Learning Representations*, 2022.
- [50] Richard Zhang, Phillip Isola, Alexei A Efros, Eli Shechtman, and Oliver Wang. The unreasonable effectiveness of deep features as a perceptual metric. In *Proceedings of the IEEE conference on computer vision and pattern recognition*, pages 586–595, 2018.
- [51] Kaiwen Zheng, Cheng Lu, Jianfei Chen, and Jun Zhu. Dpm-solver-v3: Improved diffusion ode solver with empirical model statistics. In *Thirty-seventh Conference on Neural Information Processing Systems*, 2023.
- [52] Kaiwen Zheng, Cheng Lu, Jianfei Chen, and Jun Zhu. Improved techniques for maximum likelihood estimation for diffusion odes. In *International Conference on Machine Learning*, pages 42363–42389. PMLR, 2023.
- [53] Linqi Zhou, Aaron Lou, Samar Khanna, and Stefano Ermon. Denoising diffusion bridge models. *arXiv preprint arXiv:2309.16948*, 2023.

A Related Work

Fast Sampling of Diffusion Models Fast sampling of diffusion models can be classified into training-free and training-based methods. A prevalent training-free fast sampler is the denoising diffusion implicit models (DDIMs) [40] that employ alternative non-Markovian generation processes in place of DDPMs, a discrete-time diffusion model. ScoreSDE [44] further links discrete-time DDPMs to continuous-time score-based models, unrevealing the generation process to be ordinary and stochastic differential equations (ODEs and SDEs). Subsequent training-free samplers concentrate on developing dedicated numerical solvers to the diffusion ODE or SDE, particularly Heun’s methods [21] and exponential integrators [49, 28, 29, 51, 12]. These methods typically require around 10 steps for high-quality generation. In contrast, training-based methods, particularly adversarial distillation [36] and consistency distillation [42, 23], become notable for their ability to achieve high-quality generation with just one or two steps. Developing dedicated differential equation solvers for DDBMs, or exploring bridge distillation methods, would be promising avenues for future research.

Diffusion Bridges Diffusion bridges [8, 25, 39, 53, 6, 37] are a promising generative variant of diffusion models for modeling the transport between two arbitrary distributions. One line of work is the diffusion Schrodinger bridge models [8, 37], which solves an entropy-regularized optimal transport problem between two probability distributions. However, their reliance on expensive iterative procedures has limited their application scope, particularly for high-dimensional data. Subsequent works have endeavored to enhance the tractability of the Schrodinger bridge problem by making assumptions such as paired data [25, 39, 6]. On the other hand, DDBMs [53] construct diffusion bridges via Doob’s h -transform, offering a reverse-time perspective of a diffusion process conditioned on given endpoints. This approach aligns the design spaces and training algorithms of DDBMs closely with those of score-based generative models, leading to state-of-the-art performance in image translation tasks. However, the sampling procedure of DDBMs still relies on inefficient simulations of differential equations, lacking theoretical insights to develop efficient samplers.

B Proofs

B.1 Proof of Proposition 3.1

Proof. Since $q^{(\rho)}$ in Eqn. (10) is factorized as $q^{(\rho)}(\mathbf{x}_{t_0:N-1}|\mathbf{x}_T) = q_0(\mathbf{x}_0)q^{(\rho)}(\mathbf{x}_{t_1:N-1}|\mathbf{x}_0, \mathbf{x}_T)$ where $q^{(\rho)}(\mathbf{x}_{t_1:N-1}|\mathbf{x}_0, \mathbf{x}_T) = \prod_{n=1}^{N-1} q^{(\rho)}(\mathbf{x}_{t_n}|\mathbf{x}_0, \mathbf{x}_{t_{n+1}}, \mathbf{x}_T)$, we have $q^{(\rho)}(\mathbf{x}_0|\mathbf{x}_T) = q_0(\mathbf{x}_0) = q(\mathbf{x}_0|\mathbf{x}_T)$, which proves the case for $n = 0$. For $1 \leq n \leq N - 1$, we have

$$q^{(\rho)}(\mathbf{x}_{t_n}|\mathbf{x}_T) = \int q^{(\rho)}(\mathbf{x}_{t_n}|\mathbf{x}_0, \mathbf{x}_T)q^{(\rho)}(\mathbf{x}_0|\mathbf{x}_T)d\mathbf{x}_0 \quad (21)$$

and

$$q(\mathbf{x}_{t_n}|\mathbf{x}_T) = \int q(\mathbf{x}_{t_n}|\mathbf{x}_0, \mathbf{x}_T)q(\mathbf{x}_0|\mathbf{x}_T)d\mathbf{x}_0 \quad (22)$$

Since $q^{(\rho)}(\mathbf{x}_0|\mathbf{x}_T) = q(\mathbf{x}_0|\mathbf{x}_T)$, we only need to prove $q^{(\rho)}(\mathbf{x}_{t_n}|\mathbf{x}_0, \mathbf{x}_T) = q(\mathbf{x}_{t_n}|\mathbf{x}_0, \mathbf{x}_T)$.

Firstly, when $n = N - 1$, we have $t_{n+1} = T$. Note that ρ is restricted by $\rho_{N-1} = c_{t_{N-1}}$, and Eqn. (11) becomes

$$q^{(\rho)}(\mathbf{x}_{t_{N-1}}|\mathbf{x}_0, \mathbf{x}_T) = \mathcal{N}(a_{t_{N-1}}\mathbf{x}_T + b_{t_{N-1}}\mathbf{x}_0, c_{t_{N-1}}^2\mathbf{I}) \quad (23)$$

which is exactly the same as the forward transition kernel of q in Eqn. (6). Therefore, $q^{(\rho)}(\mathbf{x}_{t_n}|\mathbf{x}_0, \mathbf{x}_T) = q(\mathbf{x}_{t_n}|\mathbf{x}_0, \mathbf{x}_T)$ holds for $n = N - 1$.

Secondly, suppose $q^{(\rho)}(\mathbf{x}_{t_n}|\mathbf{x}_0, \mathbf{x}_T) = q(\mathbf{x}_{t_n}|\mathbf{x}_0, \mathbf{x}_T)$ holds for $n = k$, we aim to prove that it holds for $n = k - 1$. Specifically, $q^{(\rho)}(\mathbf{x}_{t_{k-1}}|\mathbf{x}_0, \mathbf{x}_T)$ can be expressed as

$$\begin{aligned} q^{(\rho)}(\mathbf{x}_{t_{k-1}}|\mathbf{x}_0, \mathbf{x}_T) &= \int q^{(\rho)}(\mathbf{x}_{t_{k-1}}|\mathbf{x}_0, \mathbf{x}_{t_k}, \mathbf{x}_T)q^{(\rho)}(\mathbf{x}_{t_k}|\mathbf{x}_0, \mathbf{x}_T)d\mathbf{x}_{t_k} \\ &= \int q^{(\rho)}(\mathbf{x}_{t_{k-1}}|\mathbf{x}_0, \mathbf{x}_{t_k}, \mathbf{x}_T)q(\mathbf{x}_{t_k}|\mathbf{x}_0, \mathbf{x}_T)d\mathbf{x}_{t_k} \\ &= \int \mathcal{N}(\mathbf{x}_{t_{k-1}}; \boldsymbol{\mu}_{k-1|k}, \rho_{k-1}^2\mathbf{I})\mathcal{N}(\mathbf{x}_{t_k}; a_{t_k}\mathbf{x}_T + b_{t_k}\mathbf{x}_0, c_{t_k}^2\mathbf{I})d\mathbf{x}_{t_k} \end{aligned} \quad (24)$$

where

$$\boldsymbol{\mu}_{k-1|k} = a_{t_{k-1}} \mathbf{x}_T + b_{t_{k-1}} \mathbf{x}_0 + \sqrt{c_{t_{k-1}}^2 - \rho_{k-1}^2} \frac{\mathbf{x}_{t_k} - a_{t_k} \mathbf{x}_T - b_{t_k} \mathbf{x}_0}{c_{t_k}} \quad (25)$$

From [3] (2.115), $q^{(\rho)}(\mathbf{x}_{t_{k-1}} | \mathbf{x}_0, \mathbf{x}_T)$ is a Gaussian, denoted as $\mathcal{N}(\boldsymbol{\mu}_{k-1}, \Sigma_{k-1})$, where

$$\begin{aligned} \boldsymbol{\mu}_{k-1} &= a_{t_{k-1}} \mathbf{x}_T + b_{t_{k-1}} \mathbf{x}_0 + \sqrt{c_{t_{k-1}}^2 - \rho_{k-1}^2} \frac{a_{t_k} \mathbf{x}_T + b_{t_k} \mathbf{x}_0 - a_{t_k} \mathbf{x}_T - b_{t_k} \mathbf{x}_0}{c_{t_k}} \\ &= a_{t_{k-1}} \mathbf{x}_T + b_{t_{k-1}} \mathbf{x}_0 \end{aligned} \quad (26)$$

and

$$\begin{aligned} \Sigma_{k-1} &= \rho_{k-1}^2 \mathbf{I} + \frac{\sqrt{c_{t_{k-1}}^2 - \rho_{k-1}^2}}{c_{t_k}} c_{t_k}^2 \frac{\sqrt{c_{t_{k-1}}^2 - \rho_{k-1}^2}}{c_{t_k}} \mathbf{I} \\ &= c_{t_{k-1}}^2 \mathbf{I} \end{aligned} \quad (27)$$

Therefore, $q^{(\rho)}(\mathbf{x}_{t_{k-1}} | \mathbf{x}_0, \mathbf{x}_T) = q(\mathbf{x}_{t_{k-1}} | \mathbf{x}_0, \mathbf{x}_T) = \mathcal{N}(a_{t_{k-1}} \mathbf{x}_T + b_{t_{k-1}} \mathbf{x}_0, c_{t_{k-1}}^2 \mathbf{I})$. By mathematical deduction, $q^{(\rho)}(\mathbf{x}_{t_n} | \mathbf{x}_0, \mathbf{x}_T) = q(\mathbf{x}_{t_n} | \mathbf{x}_0, \mathbf{x}_T)$ holds for every $1 \leq n \leq N-1$, which completes the proof. \square

B.2 Proof of Proposition 3.2

Proof. Substituting Eqn. (10) and Eqn. (14) into Eqn. (15), we have

$$\begin{aligned} &\mathcal{J}^{(\rho)}(\theta) \\ &= \mathbb{E}_{q(\mathbf{x}_T)} \mathbb{E}_{q^{(\rho)}(\mathbf{x}_{t_0:N-1} | \mathbf{x}_T)} \left[\log q^{(\rho)}(\mathbf{x}_{t_1:N-1} | \mathbf{x}_0, \mathbf{x}_T) - \log p_\theta(\mathbf{x}_{t_0:N-1} | \mathbf{x}_T) \right] \\ &= \mathbb{E}_{q(\mathbf{x}_T)} \mathbb{E}_{q^{(\rho)}(\mathbf{x}_{t_0:N-1} | \mathbf{x}_T)} \left[\sum_{n=1}^{N-1} \log q^{(\rho)}(\mathbf{x}_{t_n} | \mathbf{x}_0, \mathbf{x}_{t_{n+1}}, \mathbf{x}_T) - \sum_{n=0}^{N-1} \log p_\theta(\mathbf{x}_{t_n} | \mathbf{x}_{t_{n+1}}, \mathbf{x}_T) \right] \\ &= \sum_{n=1}^{N-1} \mathbb{E}_{q(\mathbf{x}_T)} \mathbb{E}_{q^{(\rho)}(\mathbf{x}_0, \mathbf{x}_{t_{n+1}} | \mathbf{x}_T)} \left[D_{\text{KL}}(q^{(\rho)}(\mathbf{x}_{t_n} | \mathbf{x}_0, \mathbf{x}_{t_{n+1}}, \mathbf{x}_T) \parallel p_\theta(\mathbf{x}_{t_n} | \mathbf{x}_{t_{n+1}}, \mathbf{x}_T)) \right] \\ &\quad - \mathbb{E}_{q(\mathbf{x}_T)} \mathbb{E}_{q^{(\rho)}(\mathbf{x}_0, \mathbf{x}_{t_1} | \mathbf{x}_T)} [\log p_\theta(\mathbf{x}_0 | \mathbf{x}_{t_1}, \mathbf{x}_T)] \end{aligned} \quad (28)$$

where

$$\begin{aligned} &D_{\text{KL}}(q^{(\rho)}(\mathbf{x}_{t_n} | \mathbf{x}_0, \mathbf{x}_{t_{n+1}}, \mathbf{x}_T) \parallel p_\theta(\mathbf{x}_{t_n} | \mathbf{x}_{t_{n+1}}, \mathbf{x}_T)) \\ &= D_{\text{KL}}(q^{(\rho)}(\mathbf{x}_{t_n} | \mathbf{x}_0, \mathbf{x}_{t_{n+1}}, \mathbf{x}_T) \parallel q^{(\rho)}(\mathbf{x}_{t_n} | \boldsymbol{\alpha}_\theta(\mathbf{x}_{t_{n+1}}, t_{n+1}, \mathbf{x}_T), \mathbf{x}_{t_{n+1}}, \mathbf{x}_T)) \\ &= \frac{d_n^2 \|\boldsymbol{\alpha}_\theta(\mathbf{x}_{t_{n+1}}, t_{n+1}, \mathbf{x}_T) - \mathbf{x}_0\|_2^2}{2\rho_n^2} \end{aligned} \quad (29)$$

where we have denoted $d_n := b_{t_n} - \sqrt{c_{t_n}^2 - \rho_n^2} \frac{b_{t_{n+1}}}{c_{t_{n+1}}}$. Besides, we have

$$\begin{aligned} \log p_\theta(\mathbf{x}_0 | \mathbf{x}_{t_1}, \mathbf{x}_T) &= \log q^{(\rho)}(\mathbf{x}_0 | \boldsymbol{\alpha}_\theta(\mathbf{x}_{t_1}, t_1, \mathbf{x}_T), \mathbf{x}_{t_1}, \mathbf{x}_T) \\ &= \log \mathcal{N}(\boldsymbol{\alpha}_\theta(\mathbf{x}_{t_1}, t_1, \mathbf{x}_T), \rho_0^2 \mathbf{I}) \\ &= -\frac{\|\boldsymbol{\alpha}_\theta(\mathbf{x}_{t_1}, t_1, \mathbf{x}_T) - \mathbf{x}_0\|_2^2}{2\rho_0^2} + C \end{aligned} \quad (30)$$

where C is irrelevant to θ . According to Eqn. (6), the conditional score is

$$\nabla_{\mathbf{x}_t} \log q(\mathbf{x}_t | \mathbf{x}_0, \mathbf{x}_T) = -\frac{\mathbf{x}_t - a_t \mathbf{x}_T - b_t \mathbf{x}_0}{c_t^2} \quad (31)$$

Therefore,

$$\begin{aligned} &\|\boldsymbol{\alpha}_\theta(\mathbf{x}_{t_n}, t_n, \mathbf{x}_T) - \mathbf{x}_0\|_2^2 \\ &= \frac{c_{t_n}^4}{b_{t_n}^2} \left\| -\frac{\mathbf{x}_{t_n} - a_{t_n} \mathbf{x}_T - b_{t_n} \boldsymbol{\alpha}_\theta(\mathbf{x}_{t_n}, t_n, \mathbf{x}_T)}{c_{t_n}^2} - \left(-\frac{\mathbf{x}_{t_n} - a_{t_n} \mathbf{x}_T - b_{t_n} \mathbf{x}_0}{c_{t_n}^2} \right) \right\|_2^2 \\ &= \frac{c_{t_n}^4}{b_{t_n}^2} \|\boldsymbol{s}_\theta(\mathbf{x}_{t_n}, t_n, \mathbf{x}_T) - \nabla_{\mathbf{x}_{t_n}} \log q(\mathbf{x}_{t_n} | \mathbf{x}_0, \mathbf{x}_T)\|_2^2 \end{aligned} \quad (32)$$

where \mathbf{s}_θ is related to \mathbf{x}_θ by

$$\mathbf{s}_\theta(\mathbf{x}_t, t, \mathbf{x}_T) = -\frac{\mathbf{x}_t - a_t \mathbf{x}_T - b_t \mathbf{x}_\theta(\mathbf{x}_t, t, \mathbf{x}_T)}{c_t^2} \quad (33)$$

Define $d_0 = 1$, the loss $\mathcal{J}^{(\rho)}(\theta)$ is further simplified to

$$\begin{aligned} & \mathcal{J}^{(\rho)}(\theta) - C \\ &= \sum_{n=0}^{N-1} \mathbb{E}_{q(\mathbf{x}_T)q^{(\rho)}(\mathbf{x}_0, \mathbf{x}_{t_{n+1}}|\mathbf{x}_T)} \left[\frac{d_n^2 \|\mathbf{x}_\theta(\mathbf{x}_{t_{n+1}}, t_{n+1}, \mathbf{x}_T) - \mathbf{x}_0\|_2^2}{2\rho_n^2} \right] \\ &= \sum_{n=1}^N \frac{d_{n-1}^2}{2\rho_{n-1}^2} \mathbb{E}_{q(\mathbf{x}_T)q(\mathbf{x}_0|\mathbf{x}_T)q(\mathbf{x}_{t_n}|\mathbf{x}_0, \mathbf{x}_T)} [\|\mathbf{x}_\theta(\mathbf{x}_{t_n}, t_n, \mathbf{x}_T) - \mathbf{x}_0\|_2^2] \\ &= \sum_{n=1}^N \frac{d_{n-1}^2 c_{t_n}^4}{2\rho_{n-1}^2 b_{t_n}^2} \mathbb{E}_{q(\mathbf{x}_T)q(\mathbf{x}_0|\mathbf{x}_T)q(\mathbf{x}_{t_n}|\mathbf{x}_0, \mathbf{x}_T)} [\|\mathbf{s}_\theta(\mathbf{x}_{t_n}, t_n, \mathbf{x}_T) - \nabla_{\mathbf{x}_{t_n}} \log q(\mathbf{x}_{t_n}|\mathbf{x}_0, \mathbf{x}_T)\|_2^2] \end{aligned} \quad (34)$$

Compared to the training objective of DDBMs in Eqn. (9), $\mathcal{J}^{(\rho)}(\theta)$ is totally equivalent up to a constant, by concentrating on the discretized timesteps $\{t_n\}_{n=1}^N$, choosing $q(\mathbf{x}_T)q(\mathbf{x}_0|\mathbf{x}_T)$ as the paired data distribution and using the weighting function γ that satisfies $\gamma(t_n) = \frac{d_{n-1}^2 c_{t_n}^4}{2\rho_{n-1}^2 b_{t_n}^2}$. \square

B.3 Proof of Proposition 4.1

Proof. We first represent the PF-ODE (Eqn. (8))

$$d\mathbf{x}_t = \left[f(t)\mathbf{x}_t - g^2(t) \left(\frac{1}{2} \nabla_{\mathbf{x}_t} \log q(\mathbf{x}_t|\mathbf{x}_T) - \nabla_{\mathbf{x}_t} \log q_{tT}(\mathbf{x}_T|\mathbf{x}_t) \right) \right] dt \quad (35)$$

with the data predictor $\mathbf{x}_\theta(\mathbf{x}_t, t, \mathbf{x}_T)$. We replace the bridge score $\nabla_{\mathbf{x}_t} \log q(\mathbf{x}_t|\mathbf{x}_T)$ with the network $\mathbf{s}_\theta(\mathbf{x}_t, t, \mathbf{x}_T)$, which is related to $\mathbf{x}_\theta(\mathbf{x}_t, t, \mathbf{x}_T)$ by Eqn. (16). Besides, $\nabla_{\mathbf{x}_t} \log q_{tT}(\mathbf{x}_T|\mathbf{x}_t)$ can be analytically computed as

$$\begin{aligned} \nabla_{\mathbf{x}_t} \log q_{tT}(\mathbf{x}_T|\mathbf{x}_t) &= \nabla_{\mathbf{x}_t} \log \frac{q(\mathbf{x}_t|\mathbf{x}_0, \mathbf{x}_T)q(\mathbf{x}_T|\mathbf{x}_0)}{q(\mathbf{x}_t|\mathbf{x}_0)} \\ &= \nabla_{\mathbf{x}_t} \log q(\mathbf{x}_t|\mathbf{x}_0, \mathbf{x}_T) - \nabla_{\mathbf{x}_t} \log q(\mathbf{x}_t|\mathbf{x}_0) \\ &= -\frac{\mathbf{x}_t - a_t \mathbf{x}_T - b_t \mathbf{x}_0}{c_t^2} + \frac{\mathbf{x}_t - \alpha_t \mathbf{x}_0}{\sigma_t^2} \\ &= -\frac{\frac{\text{SNR}_T}{\text{SNR}_t} (\mathbf{x}_t - \frac{\alpha_t}{\alpha_T} \mathbf{x}_T)}{\sigma_t^2 (1 - \frac{\text{SNR}_T}{\text{SNR}_t})} \\ &= -\frac{a_t (\frac{\alpha_T}{\alpha_t} \mathbf{x}_t - \mathbf{x}_T)}{c_t^2} \end{aligned} \quad (36)$$

Substituting Eqn. (16) and Eqn. (36) into Eqn. (35), the PF-ODE is transformed to

$$\begin{aligned} d\mathbf{x}_t &= \left[f(t)\mathbf{x}_t - g^2(t) \left(-\frac{\mathbf{x}_t - a_t \mathbf{x}_T - b_t \mathbf{x}_\theta(\mathbf{x}_t, t, \mathbf{x}_T)}{2c_t^2} + \frac{a_t (\frac{\alpha_T}{\alpha_t} \mathbf{x}_t - \mathbf{x}_T)}{c_t^2} \right) \right] dt \\ &= \left[\left(f(t) + g^2(t) \frac{1 - 2a_t \frac{\alpha_T}{\alpha_t}}{2c_t^2} \right) \mathbf{x}_t + g^2(t) \frac{a_t}{2c_t^2} \mathbf{x}_T - g^2(t) \frac{b_t}{2c_t^2} \mathbf{x}_\theta(\mathbf{x}_t, t, \mathbf{x}_T) \right] dt \\ &= \left[\left(f(t) + \frac{g^2(t)}{\sigma_t^2} - \frac{g^2(t)}{2c_t^2} \right) \mathbf{x}_t + g^2(t) \frac{a_t}{2c_t^2} \mathbf{x}_T - g^2(t) \frac{b_t}{2c_t^2} \mathbf{x}_\theta(\mathbf{x}_t, t, \mathbf{x}_T) \right] dt \end{aligned} \quad (37)$$

On the other hand, the ODE corresponding to DBIMs (Eqn. (19)) can be expanded as

$$\frac{d\mathbf{x}_t}{c_t} - \frac{c'_t}{c_t^2} \mathbf{x}_t dt = \left[\left(\frac{a_t}{c_t} \right)' \mathbf{x}_T + \left(\frac{b_t}{c_t} \right)' \mathbf{x}_\theta(\mathbf{x}_t, t, \mathbf{x}_T) \right] dt \quad (38)$$

where we have denoted $(\cdot)' := \frac{d(\cdot)}{dt}$. Further simplification gives

$$d\mathbf{x}_t = \left[\frac{c'_t}{c_t} \mathbf{x}_t + \left(a'_t - a_t \frac{c'_t}{c_t} \right) \mathbf{x}_T + \left(b'_t - b_t \frac{c'_t}{c_t} \right) \mathbf{x}_\theta(\mathbf{x}_t, t, \mathbf{x}_T) \right] dt \quad (39)$$

The coefficients a_t, b_t, c_t are determined by the noise schedule α_t, σ_t in diffusion models. Computing their derivatives will produce terms involving $f(t), g(t)$, which are used to define the forward SDE. As revealed in diffusion models, $f(t), g(t)$ are related to α_t, σ_t by $f(t) = \frac{d \log \alpha_t}{dt}$, $g^2(t) = \frac{d\sigma_t^2}{dt} - 2 \frac{d \log \alpha_t}{dt} \sigma_t^2$. We can derive the reverse relation of α_t, σ_t and $f(t), g(t)$:

$$\alpha_t = e^{\int_0^t f(\tau) d\tau}, \quad \sigma_t^2 = \alpha_t^2 \int_0^t \frac{g^2(\tau)}{\alpha_\tau^2} d\tau \quad (40)$$

which can facilitate subsequent calculation. We first compute the derivative of a common term in a_t, b_t, c_t :

$$\left(\frac{1}{\text{SNR}_t} \right)' = \left(\frac{\sigma_t^2}{\alpha_t^2} \right)' = \frac{g^2(t)}{\alpha_t^2} \quad (41)$$

For c_t , since $c_t^2 = \sigma_t^2 (1 - \frac{\text{SNR}_T}{\text{SNR}_t})$, we have

$$\frac{c'_t}{c_t} = (\log c_t)' = \frac{1}{2} (\log c_t^2)' = \frac{1}{2} (\log \sigma_t^2 + \log (1 - \frac{\text{SNR}_T}{\text{SNR}_t}))' \quad (42)$$

where

$$(\log \sigma_t^2)' = (\log \frac{\sigma_t^2}{\alpha_t^2})' + (\log \alpha_t^2)' = \frac{g^2(t)}{\alpha_t^2} \frac{\alpha_t^2}{\sigma_t^2} + 2f(t) = \frac{g^2(t)}{\sigma_t^2} + 2f(t) \quad (43)$$

and

$$(\log (1 - \frac{\text{SNR}_T}{\text{SNR}_t}))' = -\frac{\text{SNR}_T}{1 - \frac{\text{SNR}_T}{\text{SNR}_t}} \left(\frac{1}{\text{SNR}_t} \right)' = -\frac{\text{SNR}_T}{c_t^2} \sigma_t^2 \frac{g^2(t)}{\alpha_t^2} = -\frac{g^2(t)}{c_t^2} \frac{\text{SNR}_T}{\text{SNR}_t} \quad (44)$$

Substituting Eqn. (43) and Eqn. (44) into Eqn. (42), and using the relation $\frac{\text{SNR}_T}{\text{SNR}_t} = 1 - \frac{c_t^2}{\sigma_t^2}$, we have

$$\frac{c'_t}{c_t} = f(t) + \frac{g^2(t)}{2\sigma_t^2} - \frac{g^2(t)}{2c_t^2} \frac{\text{SNR}_T}{\text{SNR}_t} = f(t) + \frac{g^2(t)}{\sigma_t^2} - \frac{g^2(t)}{2c_t^2} \quad (45)$$

For a_t , since $a_t = \frac{\alpha_t}{\alpha_T} \frac{\text{SNR}_T}{\text{SNR}_t}$, we have

$$\frac{a'_t}{a_t} = (\log a_t)' = (\log \alpha_t)' + (\log \frac{\text{SNR}_T}{\text{SNR}_t})' = f(t) + \text{SNR}_T \frac{g^2(t)}{\alpha_t^2} = f(t) + \frac{g^2(t)}{\sigma_t^2} \quad (46)$$

For b_t , since $b_t = \alpha_t (1 - \frac{\text{SNR}_T}{\text{SNR}_t})$, we have

$$\frac{b'_t}{b_t} = (\log b_t)' = (\log \alpha_t)' + (\log (1 - \frac{\text{SNR}_T}{\text{SNR}_t}))' = f(t) - \frac{g^2(t)}{c_t^2} \frac{\text{SNR}_T}{\text{SNR}_t} = f(t) + \frac{g^2(t)}{\sigma_t^2} - \frac{g^2(t)}{c_t^2} \quad (47)$$

Therefore,

$$a'_t - a_t \frac{c'_t}{c_t} = a_t \left(\frac{a'_t}{a_t} - \frac{c'_t}{c_t} \right) = \frac{g^2(t)}{2c_t^2} a_t \quad (48)$$

and

$$b'_t - b_t \frac{c'_t}{c_t} = b_t \left(\frac{b'_t}{b_t} - \frac{c'_t}{c_t} \right) = -\frac{g^2(t)}{2c_t^2} b_t \quad (49)$$

Substituting Eqn. (45), Eqn. (48) and Eqn. (49) into the ODE of DBIMs in Eqn. (39), we obtain exactly the PF-ODE in Eqn. (37). \square

C Markov Property of the Generalized Diffusion Bridges

We aim to analyze the Markov property of the forward process corresponding to our generalized diffusion bridge in Section 3.1. The forward process is expressed as

$$q^{(\rho)}(\mathbf{x}_{t_{n+1}}|\mathbf{x}_0, \mathbf{x}_{t_n}, \mathbf{x}_T) = \frac{q^{(\rho)}(\mathbf{x}_{t_n}|\mathbf{x}_0, \mathbf{x}_{t_{n+1}}, \mathbf{x}_T)q^{(\rho)}(\mathbf{x}_{t_{n+1}}|\mathbf{x}_0, \mathbf{x}_T)}{q^{(\rho)}(\mathbf{x}_{t_n}|\mathbf{x}_0, \mathbf{x}_T)} \quad (50)$$

where $q^{(\rho)}(\mathbf{x}_{t_n}|\mathbf{x}_0, \mathbf{x}_{t_{n+1}}, \mathbf{x}_T)$ is defined in Eqn. (11) as

$$q^{(\rho)}(\mathbf{x}_{t_n}|\mathbf{x}_0, \mathbf{x}_{t_{n+1}}, \mathbf{x}_T) = \mathcal{N}\left(a_{t_n} \mathbf{x}_T + b_{t_n} \mathbf{x}_0 + \frac{\sqrt{c_{t_n}^2 - \rho_n^2} \mathbf{x}_{t_{n+1}} - a_{t_{n+1}} \mathbf{x}_T - b_{t_{n+1}} \mathbf{x}_0}{c_{t_{n+1}}}, \rho_n^2 \mathbf{I}\right). \quad (51)$$

Due to the marginal preservation property (Proposition 3.1), we have $q^{(\rho)}(\mathbf{x}_{t_{n+1}}|\mathbf{x}_0, \mathbf{x}_T) = q(\mathbf{x}_{t_{n+1}}|\mathbf{x}_0, \mathbf{x}_T)$ and $q^{(\rho)}(\mathbf{x}_{t_n}|\mathbf{x}_0, \mathbf{x}_T) = q(\mathbf{x}_{t_n}|\mathbf{x}_0, \mathbf{x}_T)$, where $q(\mathbf{x}_t|\mathbf{x}_0, \mathbf{x}_T) = \mathcal{N}(a_t \mathbf{x}_T + b_t \mathbf{x}_0, c_t^2 \mathbf{I})$ is the forward transition kernel in Eqn. (6). To identify whether $q^{(\rho)}(\mathbf{x}_{t_{n+1}}|\mathbf{x}_0, \mathbf{x}_{t_n}, \mathbf{x}_T)$ is Markovian, we only need to examine the dependence of $\mathbf{x}_{t_{n+1}}$ on \mathbf{x}_0 . To this end, we proceed to derive conditions under which $\nabla_{\mathbf{x}_{t_{n+1}}} \log q^{(\rho)}(\mathbf{x}_{t_{n+1}}|\mathbf{x}_0, \mathbf{x}_T)$ involves terms concerning \mathbf{x}_0 .

Specifically, $\nabla_{\mathbf{x}_{t_{n+1}}} \log q^{(\rho)}(\mathbf{x}_{t_{n+1}}|\mathbf{x}_0, \mathbf{x}_T)$ can be calculated as

$$\begin{aligned} & \nabla_{\mathbf{x}_{t_{n+1}}} \log q^{(\rho)}(\mathbf{x}_{t_{n+1}}|\mathbf{x}_0, \mathbf{x}_T) \\ &= \nabla_{\mathbf{x}_{t_{n+1}}} \log q^{(\rho)}(\mathbf{x}_{t_n}|\mathbf{x}_0, \mathbf{x}_{t_{n+1}}, \mathbf{x}_T) + \nabla_{\mathbf{x}_{t_{n+1}}} \log q^{(\rho)}(\mathbf{x}_{t_{n+1}}|\mathbf{x}_0, \mathbf{x}_T) \\ &= -\frac{\sqrt{c_{t_n}^2 - \rho_n^2} (a_{t_n} \mathbf{x}_T + b_{t_n} \mathbf{x}_0) + \sqrt{c_{t_n}^2 - \rho_n^2} \frac{\mathbf{x}_{t_{n+1}} - a_{t_{n+1}} \mathbf{x}_T - b_{t_{n+1}} \mathbf{x}_0}{c_{t_{n+1}}}}{c_{t_{n+1}} \rho_n^2} \\ & \quad - \frac{\mathbf{x}_{t_{n+1}} - a_{t_{n+1}} \mathbf{x}_T - b_{t_{n+1}} \mathbf{x}_0}{c_{t_{n+1}}^2} \\ &= \frac{b_{t_{n+1}} c_{t_n}^2 - b_{t_n} c_{t_{n+1}} \sqrt{c_{t_n}^2 - \rho_n^2}}{c_{t_{n+1}}^2 \rho_n^2} \mathbf{x}_0 + C(\mathbf{x}_{t_n}, \mathbf{x}_{t_{n+1}}, \mathbf{x}_T) \end{aligned} \quad (52)$$

where $C(\mathbf{x}_{t_n}, \mathbf{x}_{t_{n+1}}, \mathbf{x}_T)$ are terms irrelevant to \mathbf{x}_0 . Therefore,

$$\begin{aligned} q^{(\rho)}(\mathbf{x}_{t_{n+1}}|\mathbf{x}_0, \mathbf{x}_{t_n}, \mathbf{x}_T) \text{ is Markovian} &\iff \frac{b_{t_{n+1}} c_{t_n}^2 - b_{t_n} c_{t_{n+1}} \sqrt{c_{t_n}^2 - \rho_n^2}}{c_{t_{n+1}}^2 \rho_n^2} = 0 \\ &\iff \rho_n = \sigma_{t_n} \sqrt{1 - \frac{\text{SNR}_{t_{n+1}}}{\text{SNR}_{t_n}}} \end{aligned} \quad (53)$$

which is exactly a boundary choice of the variance parameter ρ . Under the other boundary choice $\rho_n = 0$ and intermediate ones satisfying $0 < \rho_n < \sigma_{t_n} \sqrt{1 - \frac{\text{SNR}_{t_{n+1}}}{\text{SNR}_{t_n}}}$, the forward process $q^{(\rho)}(\mathbf{x}_{t_{n+1}}|\mathbf{x}_0, \mathbf{x}_{t_n}, \mathbf{x}_T)$ is non-Markovian.

D Experiment Details

D.1 Model Details

DDBMs and DBIMs are assessed using the same trained diffusion bridge models. For image translation tasks, we directly adopt the pretrained checkpoints provided by DDBMs. The data prediction model $\mathbf{x}_\theta(\mathbf{x}_t, t, \mathbf{x}_T)$ mentioned in the main text is parameterized by the network \mathbf{F}_θ as $\mathbf{x}_\theta(\mathbf{x}_t, t, \mathbf{x}_T) = c_{\text{skip}}(t) \mathbf{x}_t + c_{\text{out}}(t) \mathbf{F}_\theta(c_{\text{in}}(t) \mathbf{x}_t, c_{\text{noise}}(t), \mathbf{x}_T)$, where

$$\begin{aligned} c_{\text{in}}(t) &= \frac{1}{\sqrt{a_t^2 \sigma_T^2 + b_t^2 \sigma_0^2 + 2a_t b_t \sigma_{0T} + c_t}}, & c_{\text{out}}(t) &= \sqrt{a_t^2 (\sigma_T^2 \sigma_0^2 - \sigma_{0T}^2) + \sigma_0^2 c_t c_{\text{in}}(t)} \\ c_{\text{skip}}(t) &= (b_t \sigma_0^2 + a_t \sigma_{0T}) c_{\text{in}}^2(t), & c_{\text{noise}}(t) &= \frac{1}{4} \log t \end{aligned} \quad (54)$$

and

$$\sigma_0^2 = \text{Var}[\mathbf{x}_0], \sigma_T^2 = \text{Var}[\mathbf{x}_T], \sigma_{0T} = \text{Cov}[\mathbf{x}_0, \mathbf{x}_T] \quad (55)$$

For the image inpainting task on ImageNet 256×256 with 128×128 center mask, DDBMs do not provide available checkpoints. Therefore, we train a new model from scratch using the noise schedule of I²SB [25]. The network is initialized from the pretrained class-conditional diffusion model on ImageNet 256×256 provided by [10], while additionally conditioned on \mathbf{x}_T . The data prediction model in this case is parameterized by the network \mathbf{F}_θ as $\mathbf{x}_\theta(\mathbf{x}_t, t, \mathbf{x}_T) = \mathbf{x}_t - \sigma_t \mathbf{F}_\theta(\mathbf{x}_t, t, \mathbf{x}_T)$ and trained by minimizing the loss $\mathcal{L}(\theta) = \mathbb{E}_{t, \mathbf{x}_0, \mathbf{x}_T} \left[\frac{1}{\sigma_t^2} \|\mathbf{x}_\theta(\mathbf{x}_t, t, \mathbf{x}_T) - \mathbf{x}_0\|_2^2 \right]$. We train the model on 8 NVIDIA A800 GPU cards with a batch size of 256 for 400k iterations, which takes around 19 days.

D.2 Sampling Details

We elaborate on the sampling configurations of different approaches, including the choice of timesteps $\{t_i\}_{i=0}^N$ and details of the samplers. In this work, we adopt $t_{\min} = 0.0001$ and $t_{\max} = 1$ following [53]. For the DDBM baseline, we use the hybrid, high-order Heun sampler proposed in their work with an Euler step ratio of 0.33, which is the best performing configuration for the image-to-image translation task. We use the same timesteps distributed according to EDM [21]’s scheduling $(t_{\max}^{1/\rho} + \frac{i}{N}(t_{\min}^{1/\rho} - t_{\max}^{1/\rho}))^\rho$, consistent with the official implementation of DDBM. For DBIM, since the initial sampling step is distinctly forced to be stochastic, we specifically set it to transition from t_{\max} to $t_{\max} - 0.0001$, and employ a simple uniformly distributed timestep scheme in $[t_{\min}, t_{\max} - 0.0001]$ for the remaining timesteps, across all settings. For interpolation experiments, to enhance diversity, we increase the step size of the first step from 0.0001 to 0.01.

D.3 License

Table 6: The used datasets, codes and their licenses.

Name	URL	Citation	License
Edges→Handbags	https://github.com/junyanz/pytorch-CycleGAN-and-pix2pix	[19]	BSD
DIODE-Outdoor	https://diode-dataset.org/	[46]	MIT
ImageNet	https://www.image-net.org	[9]	\
Guided-Diffusion	https://github.com/openai/guided-diffusion	[10]	MIT
I ² SB	https://github.com/NVlabs/I2SB	[25]	CC-BY-NC-SA-4.0
DDBM	https://github.com/alexzhou907/DDBM	[53]	\

We list the used datasets, codes and their licenses in Table 6.

E Additional Samples

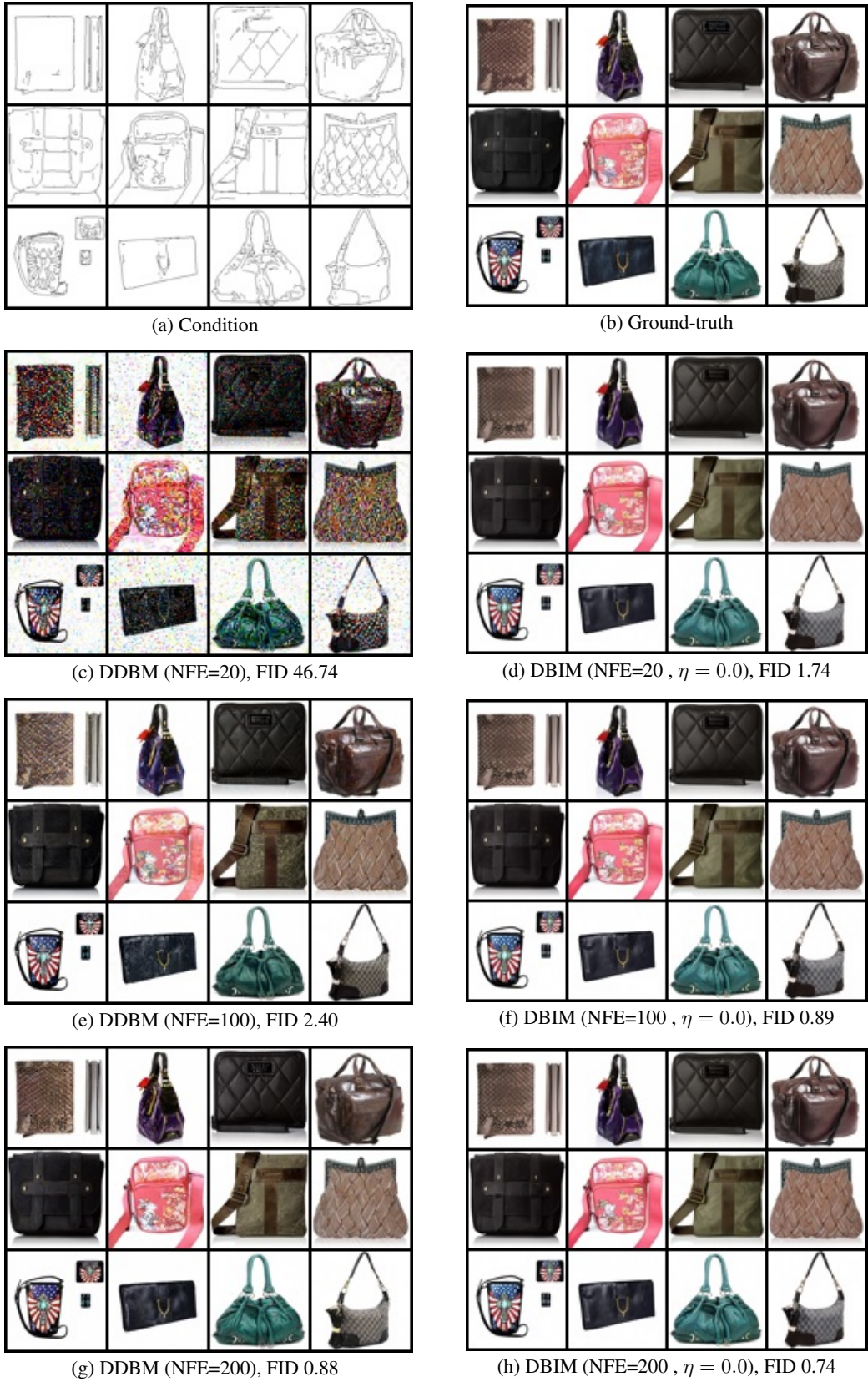
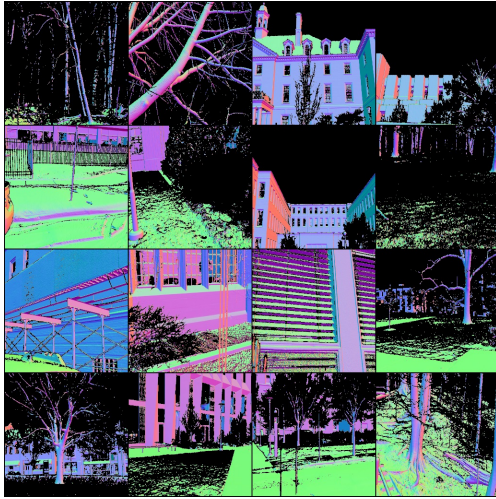


Figure 6: Edges \rightarrow Handbags samples on the translation task.



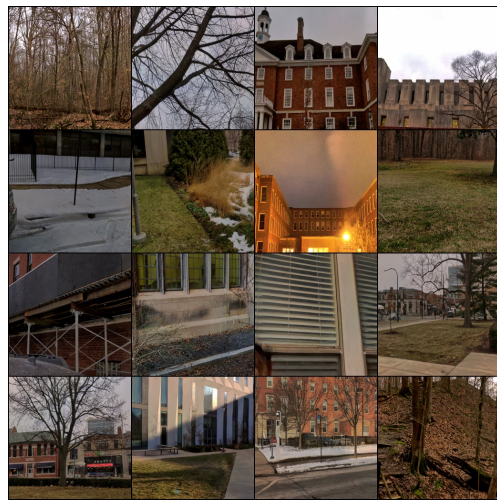
(a) Condition



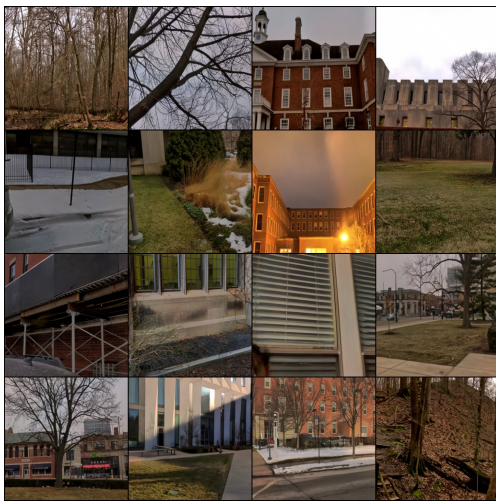
(b) Ground-truth



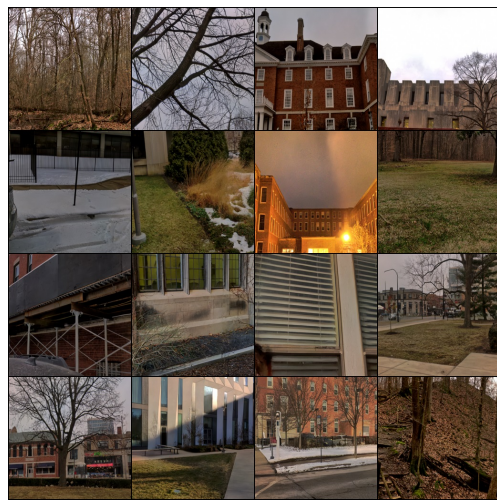
(c) DDBM (NFE=20), FID 41.03



(d) DDBM (NFE=500), FID 2.26

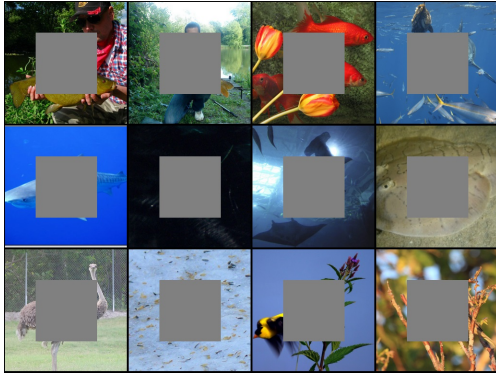


(e) DBIM (NFE=20, $\eta = 0.0$), FID 4.99



(f) DBIM (NFE=200, $\eta = 0.0$), FID 2.27

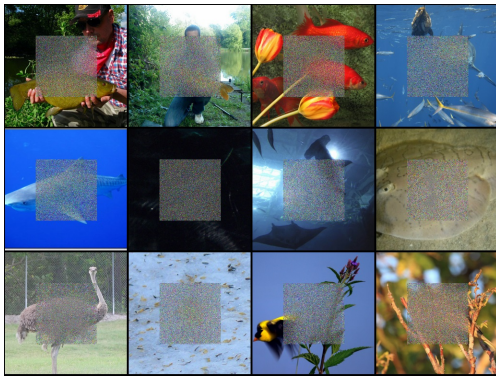
Figure 7: DIODE-Outdoor samples on the translation task.



(a) Condition



(b) Ground-truth



(c) DDBM (NFE=10), FID 57.18



(d) DDBM (NFE=500), FID 4.27



(e) DBIM (NFE=10, $\eta = 0.0$), FID 4.62



(f) DBIM (NFE=100, $\eta = 0.0$), FID 3.95



(g) DBIM (NFE=100, $\eta = 0.8$), FID 3.88



(h) DBIM (NFE=500, $\eta = 1.0$), FID 3.83

Figure 8: ImageNet 256×256 samples on the inpainting task with center 128×128 mask.